NASA/CR-1998 208311

THE STRUCTURE AND DYNAMICS OF THE SOLAR CORONA

NASA SPACE PHYSICS THEORY CONTRACT NAS5-96081

FIRST YEAR PROGRESS REPORT

Covering the period July 26, 1996 to July 15, 1997

Submitted by:

Zoran Mikić
Principal Investigator
Science Applications International Corporation
10260 Campus Point Drive
San Diego, CA 92121

June 5, 1998

FIRST YEAR PROGRESS REPORT

This report covers technical progress during the first year of the NASA Space Physics Theory contract "The Structure and Dynamics of the Solar Corona," NAS5-96081, between NASA and Science Applications International Corporation, and covers the period July 26, 1996 to July 16, 1997. Under this contract SAIC, the University of California, Irvine (UCI), and the Jet Propulsion Laboratory (JPL), have conducted research into theoretical modeling of active regions, the solar corona, and the inner heliosphere, using the MHD model. During the period covered by this report we have published 26 articles in the scientific literature. These publications are listed in Section 4 of this report. In the Appendix we have attached reprints of selected articles.

1. INTRODUCTION

An important goal of NASA's space physics program is to develop a quantitative understanding of the Earth's plasma environment. The Sun, as the driver of terrestrial geomagnetic disturbances, has an all-important influence on the Earth. This Sun-Earth connection, dubbed "space weather," has recently been recognized as an important activity for the space science community.

Our program centers around the theoretical modeling of active regions, the solar corona, and the inner heliosphere, using the MHD model. This capability allows us to compare our model quantitatively with many observations, including interplanetary scintillation (IPS) and *in situ* spacecraft measurements of the solar wind, and coronal emission (e.g., white light, radio, SOHO EIT and UVCS).

2. ACHIEVEMENTS

In this section we summarize the accomplishments made by our group during the first year of our Space Physics Theory Program contract. The descriptions are primarily intended to illustrate our principal results. A full account can be found in the referenced publications.

2.1. Modeling the Large-Scale Structure of the Corona and Inner Heliosphere

Our description of the solar corona and inner heliosphere is based on numerical solutions of the MHD equations. We have extended the state-of-the-art in coronal modeling in three principal areas: we have brought in geometrical realism (by extending 1D and 2D models to 2D and 3D models, respectively); we have used more sophisticated physics, including an improved description of energy flow; and we have used solar observations, principally the measured photospheric magnetic field, to make it possible to directly compare our calculations with solar observations.

2.1.1. An Improved MHD Model of the Solar Corona and Inner Heliosphere

Our modeling of the global properties of the solar corona relies on the MHD model to describe the interaction of the solar wind with coronal magnetic fields. In order to simplify the description, we initially used a "polytropic model," in which an adiabatic energy equation with a reduced polytropic index γ (i.e., smaller than 5/3) is used (Parker 1963). This is a crude way of modeling the complicated thermodynamics in the corona with a simple energy equation. The

TABLE OF CONTENTS

primary motivation for using a reduced γ is the fact that the temperature in the corona does not vary substantially, since the limit $\gamma \rightarrow 1$ corresponds to an isothermal plasma. A typical choice is $\gamma = 1.05$. Comparisons of our results with coronal observations indicate that while this model matches many features of the corona, it is not accurate enough to quantitatively reproduce the properties of the corona and solar wind. In particular, this simple model fails to reproduce the fast (~ 800 km/s) and slow (~ 400 km/s) solar wind streams that are measured at 1 AU, nor does it reproduce the contrast in density and temperature that is observed between streamers and coronal holes.

We have improved this aspect of the formulation by modeling in detail the physical mechanisms that describe the transport of energy in the corona and solar wind. One-dimensional MHD models have been quite successful, despite their obvious geometrical limitations, in describing this interaction and in comparisons with spacecraft solar wind measurements (Withbroe 1988; Habbal *et al.* 1995). We have improved the energy equation in our model to include the effects of parallel thermal conduction, radiation loss, parameterized coronal heating, and Alfvén wave acceleration. Our improved model is based on the following MHD equations:

$$\nabla \times \mathbf{B} = \frac{4\pi}{c}\mathbf{J} , \tag{1}$$

$$\nabla \times \mathbf{E} = -\frac{1}{c}\frac{\partial \mathbf{B}}{\partial t} , \tag{2}$$

$$\mathbf{E} + \frac{1}{c}\mathbf{v} \times \mathbf{B} = \eta \mathbf{J} , \tag{3}$$

$$\frac{\partial \rho}{\partial t} + \nabla \cdot (\rho \mathbf{v}) = 0 , \tag{4}$$

$$\rho\left(\frac{\partial \mathbf{v}}{\partial t} + \mathbf{v} \cdot \nabla \mathbf{v}\right) = \frac{1}{c}\mathbf{J} \times \mathbf{B} - \nabla p - \nabla p_w + \rho \mathbf{g} + \nabla \cdot (\nu \rho \nabla \mathbf{v}) , \tag{5}$$

$$\frac{\partial p}{\partial t} + \nabla \cdot (p\mathbf{v}) = (\gamma - 1)\left(-p\nabla \cdot \mathbf{v} + S\right) , \tag{6}$$

$$S = -\nabla \cdot \mathbf{q} - n_e n_p Q(T) + H_{\mathrm{ch}} + H_{\mathrm{d}} + D , \tag{7}$$

where $\mathbf{B}$ is the magnetic field, $\mathbf{J}$ is the current density, $\mathbf{E}$ is the electric field, ρ, $\mathbf{v}$, p, and T are the plasma mass density, velocity, pressure, and temperature, and the wave pressure p_w represents the acceleration due to Alfvén waves. The gravitational acceleration is $\mathbf{g}$, $\gamma = 5/3$ is the ratio of specific heats, η is the resistivity, ν is the viscosity, H_{ch} is the coronal heating source, D is the Alfvén wave dissipation term, n_e and n_p are the electron and proton density, and $Q(T)$ is the radiation loss function (Rosner *et al.* 1978). The term $H_{\mathrm{d}} = \eta J^2 + \nu \nabla \mathbf{v} : \nabla \mathbf{v}$ represents heating due to viscous and resistive dissipation. In the collisional regime (below ~ $10R_s$), the heat flux is $\mathbf{q} = -\kappa_{\|} \hat{\mathbf{b}} \hat{\mathbf{b}} \cdot \nabla T$, where $\hat{\mathbf{b}}$ is the unit vector along $\mathbf{B}$, and $\kappa_{\|} = 9 \times 10^7\, T^{5/2}$ is the Spitzer value of the parallel thermal conductivity. In the collisionless regime (beyond ~ $10R_s$), the heat flux is given by $\mathbf{q} = \alpha n_e k T \mathbf{v}$, where α is a parameter (Hollweg 1978). Since it is presently not known

in detail what heats the solar corona, the coronal heating source H_{ch} is a parameterized function. A typical form is

$$H_{ch} = H_0(\theta) \exp\left[-(r - R_s)/\lambda(\theta)\right] , \tag{8}$$

where $H_0(\theta)$ expresses the latitudinal variation of the volumetric heating, and $\lambda(\theta)$ expresses the latitudinal variation of the heating function scale length. [In practice, the variation is expressed in terms of the magnetic topology (i.e., a proxy for the open and closed field regions) rather than the latitude θ.] Note that the simplified polytropic model is obtained by setting $S = 0$ in Eq. (6), $p_w = 0$ in Eq. (5), and $\gamma = 1.05$.

Since the acceleration of the solar wind by Alfvén waves occurs on a spatial and time scale that is below the spatial and time resolution of our global numerical model, the wave pressure p_w is evolved using an equation for the time-space averaged Alfvén wave energy density ε (Jacques 1977),

$$\frac{\partial \varepsilon}{\partial t} + \nabla \cdot \mathbf{F} = \mathbf{v} \cdot \nabla p_w - D , \tag{9}$$

where $\mathbf{F} = (\frac{3}{2}\mathbf{v} + \mathbf{v}_A)\varepsilon$ is the Alfvén wave energy flux, $v_A = B/\sqrt{4\pi\rho}$ is the Alfvén speed, and $p_w = \frac{1}{2}\varepsilon$. The Alfvén wave velocity is $\mathbf{v}_A = \pm\hat{\mathbf{b}}v_A$; in a multi-dimensional implementation, it is necessary to transport two Alfvén wave fields (waves parallel and antiparallel to $\mathbf{B}$), which are combined to give ε. The Alfvén wave energy density ε is related to the space-time average of the fluctuating component of the magnetic field δB by $\varepsilon = <\delta B^2>/4\pi$. The dissipation term D expresses the nonlinear dissipation of Alfvén waves in interplanetary space and is modeled phenomenologically (Hollweg 1978).

We use the following boundary conditions (Mikić & Linker 1994; Linker *et al.* 1996; Linker & Mikić 1997). The radial magnetic field is specified at the solar surface $r = R_s$ (e.g., from synoptic magnetic field observations, or from full-disk magnetograms). The boundary conditions on the velocity are determined from the characteristic equations along $\mathbf{B}$. The boundary $r = R_s$ is chosen to be at the top of the transition region, at a given temperature (say $T_0 = 500{,}000°K$). The density at $r = R_s$ is determined by balancing radiation loss, thermal conduction, and heating within the chromosphere and transition region (Withbroe 1988). In this formulation, the only boundary conditions required from observations at the base of the corona $r = R_s$ are on the radial magnetic field. [In the polytropic model, in contrast, we specify a uniform density in the open-field regions and a uniform temperature at the base of the corona.]

We have developed a three-dimensional code to solve MHD equations (1)–(9) in spherical coordinates (r,θ,ϕ). This code is described in part by Mikić and Linker (1994) and by Lionello, Mikić, and Schnack (1998). This code has been used extensively to model the 2D and 3D corona, including the solar wind, differential solar rotation, simulation of the interplanetary medium (from the Sun to 1 AU), the effect of emerging flux, coronal mass ejections, and the long-term evolution of the solar corona and heliospheric current sheet. In the following sections we describe the application of this code to several problems of interest in large-scale coronal physics.

This improved model makes it possible to study the solar wind from its origin in the low corona to its expansion into interplanetary space. It is presently being used in 2D, and will soon be

implemented in 3D. We still routinely employ the polytropic model (currently the only model we use in 3D) when a qualitative description of the corona is sufficient, since the full model requires considerably increased computational resources. With the 3D improved model it will be possible to directly compare model results with *in situ* spacecraft measurements.

Even with these improvements to the energy equation, it must be recognized that a single-fluid description (inherent in the MHD model) is still a considerable approximation to the state of the corona. In particular, recent SOHO observations imply that the electron temperature is considerably lower in the corona than the ion temperature. One-dimensional models (e.g., Li, Esser, & Habbal 1997) have extended the theory to multiple fluids. Our present philosophy is to include the effects of multi-dimensional geometry in a single-fluid model first, since this effect has not been explored fully. Eventually our formalism can be extended to include multiple fluids.

2.1.2. Comparison with Eclipse Observations

We have by now established a "tradition" of using our 3D MHD model to predict the state of the corona during forthcoming total solar eclipses. Our first attempt was a comparison that was performed subsequent to the eclipse of November 3, 1994. (Our eclipse comparisons can be seen on our Web page, http://iris023.saic.com:8000/corona/modeling.html.) Since then, we have made two *predictions*, before the actual eclipse date, using magnetic field data from the previous solar rotation. Our success has been reassuring, primarily because these eclipses occurred close to solar minimum, when the large-scale structure of the Sun changes slowly between solar rotations. In Figure 1 we compare our comparisons and predictions to observations of the eclipses of November 3, 1994, observed in Chile, October 24, 1995, observed in Vietnam, and March 9, 1997, observed in Siberia.

To perform these calculations, we used Kitt Peak National Observatory and Wilcox Solar Observatory synoptic magnetic field maps to specify the radial magnetic field at the photosphere as a boundary condition for our 3D MHD solutions to compute the state of the coronal plasma, including the density and magnetic field (Mikić & Linker 1996). The simulated polarization brightness from our simulation is computed by integrating the electron density along the line of sight in the plane of the sky. Comparisons with Mauna Loa MK3 coronagraph observations during the solar rotation surrounding the eclipse have confirmed that the basic large-scale three-dimensional structure of the streamer belt has been captured in the model.

2.1.3. MHD Modeling for the Ulysses Fast Latitude Scan

We have also applied our model to Ulysses observations during the fast latitude scan (Feb.–Apr., 1995). We used the MHD model to deduce the solar origin of plasma observed at Ulysses. HCS crossings from the MHD model were compared with those from the source-surface model and Ulysses measurements. Figure 2 shows that the polarity of the magnetic field predicted by the MHD model generally matches Ulysses observations. It is apparent that the Ulysses data shows a general trend: the fast wind comes from deeper within coronal holes than the slow wind . Full details are given by Neugebauer *et al.* (1998).

Eclipse Comparisons

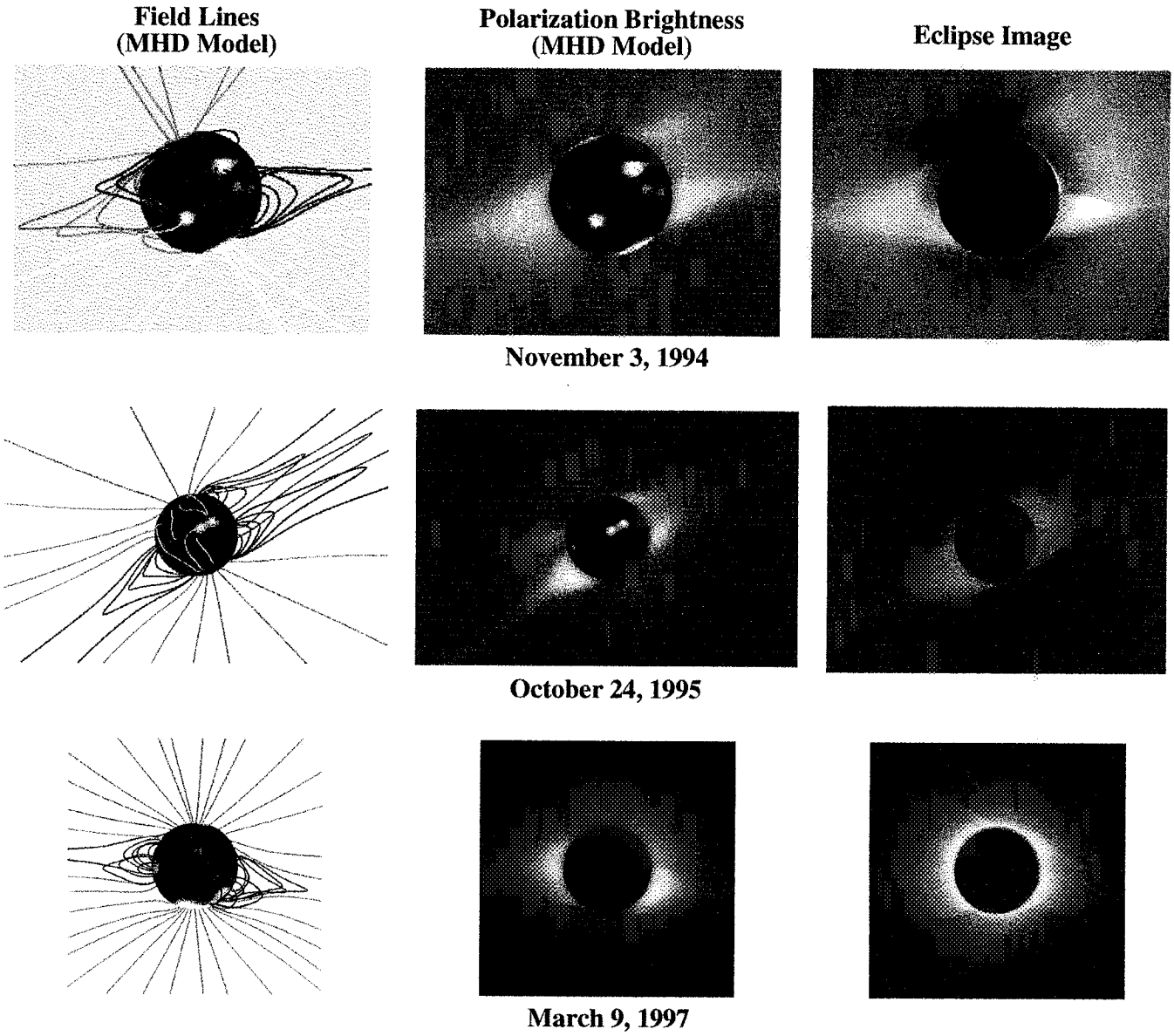

Figure 1. Comparison of MHD computations of the solar corona with total solar eclipse observations. The 1994 eclipse image is courtesy of the the High Altitude Observatory, NCAR, Boulder, Colorado, USA. NCAR is sponsored by NSF. The 1995 eclipse image is courtesy of F. Diego and S. Koutchmy. The 1997 eclipse image is courtesy of the Eclipse Team of Meisei University, lead by Professor Eijiro Hiei of Meisei University and the National Astronomical Observatory of Japan.

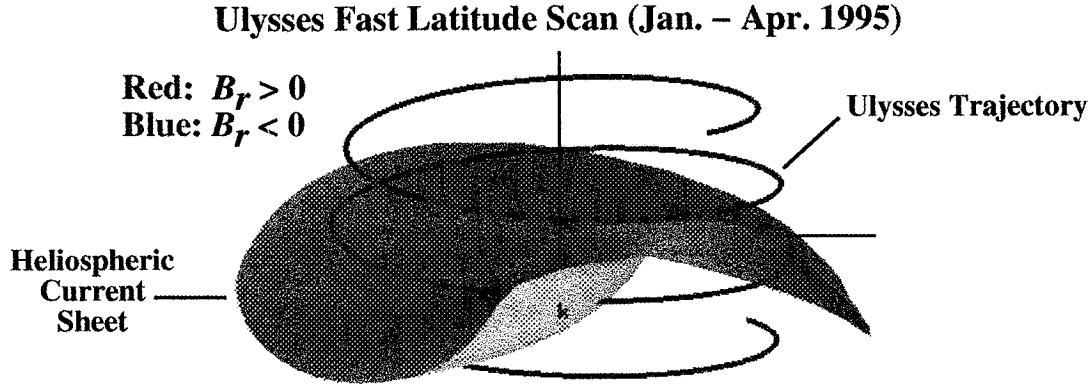

Figure 2. Heliospheric current sheet for Carrington rotations 1892–1894, showing the trajectory of Ulysses, in the rotating frame of the Sun. The color of the trajectory indicates the polarity of the magnetic field. The measured large–scale polarity of the magnetic field is consistent wth that predicted by the MHD model (positive above the HCS, negative below).

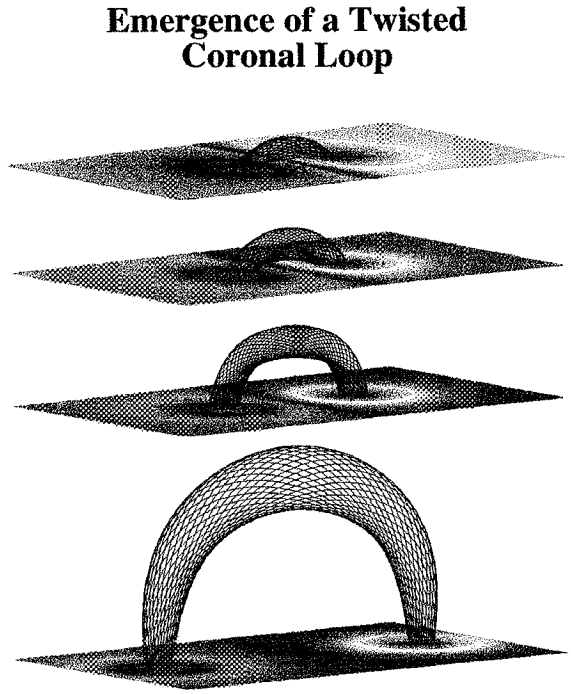

Figure 3. Emergence of a current–carrying coronal loop from below the photosphere. Note that the field lines twist around the axis of the loop as they traverse from one footpoint to the other.

2.1.4. Modeling the Solar Wind

The improvements to the energy equation described in Section 2.1.1 were implemented primarily to model the properties of the solar wind. We have performed extensive modeling in 2D (axisymmetric) geometry in order to self-consistently model the solar wind from its origins in the low corona to its expansion into interplanetary space. In order to match observed fast and slow wind velocities, mass fluxes, and densities at 1 AU, the coronal heating scale length (λ in Eq. 9) needs to be shorter in the streamer belt than near the poles, consistent with Withbroe (1988). We have also found that it is necessary to specify an Alfvén wave flux in order to match the fast wind speed. Our results show promising matches with generic *in situ* observations of the fast and slow solar wind, as well as the observed properties in the low corona (density and temperature contrasts between the streamer belt and coronal holes). This model is directly extensible to 3D geometry.

2.1.5. Correlation of Flux Tube Expansion with Solar Wind Velocity

Past observational work has demonstrated an anti-correlation between coronal magnetic flux-tube expansion and solar wind speed (Wang & Sheeley 1990). We have compared solar wind velocities from Ulysses/SWOOPS to magnetic expansion factors computed from a 3D MHD model for Carrington rotation 1892 (during the Ulysses "fast latitude scan"; See Sec. 2.1.3). The comparison was made for a period during which Ulysses saw both fast and slow solar wind. We found that the MHD model showed slower wind from an equatorial coronal hole with a larger expansion factor than from a coronal hole with a smaller expansion factor, consistent with previous observations. However, in general, we found the correlation between solar wind speed and expansion factor to be very weak (Liewer *et al.* 1996).

2.2. Coronal Mass Ejections

2.2.1. Eruption of 3D Streamers by Photospheric Shear

As an extension of our study of the disruption of axisymmetric arcades (Mikić & Linker 1994) and helmet streamers (Linker & Mikić 1995), we studied the evolution of helmet streamers in 3D geometry. We found that a similar disruption occurs in 3D geometry, and that the ejected plasmoid has a large-scale longitudinal extent, as seen in LASCO observations in which CMEs appear to leave the Sun on both limbs simultaneously. A discussion of the role of photospheric shear in initiating CMEs is given by Mikić & Linker (1997). The propagation of the ejection to 1 AU is discussed by Linker & Mikić (1997).

2.3. Three-Dimensional Active Region Modeling

2.3.1. Emergence of Twisted Coronal Loops

In a previous study we investigated the properties of coronal loops that were formed dynamically by twisting motions in the photosphere (Van Hoven, Mok, & Mikić 1995). Using the new emerging flux capability in our 3D Cartesian MHD code, we have studied the emergence of twisted (i.e., current-carrying) magnetic flux in active regions (Leka *et al.* 1996). Since we do not wish to simulate the dynamics of the convection zone, we take a phenomenological approach to flux emergence: we specify time-dependent profiles of the normal magnetic field, B_z and the

normal current density, J_z as boundary conditions at the base of the corona ($z = 0$). The profiles B_z and J_z are specified by applying a tangential electric field at the boundary.

This formalism gives us considerable flexibility in specifying the properties of the emerging magnetic flux and current in order to model the observed magnetic structures in the solar atmosphere. (The profiles B_z and J_z could be inferred from vector magnetograph observations.) By appropriately specifying B_z and J_z we have modeled the emergence of twisted magnetic field loops (Mok, Van Hoven, & Mikić 1997). Figure 3 shows the emergence of a single magnetic loop. Note that the field lines are twisted, showing that the loop carries current. The loop is non-planar and truly three-dimensional, displaying an *S*-shape when viewed from above.

2.3.2. Comparison with Radio Observations

In a collaboration with J. Lee (U. Maryland) we compared a force-free coronal magnetic field extrapolation (Mikić & McClymont 1994; Mikić, Linker, & Schnack 1996), determined from vector magnetograph observations of active region 6615 in May 1991, with observed radio emission. We found that force-free fields match the radio emission better than potential fields do (Lee *et al.* 1998a,c). The radio data and magnetic field model were used to deduce the density in the active region, and to compare it to observations (Lee *et al.* 1998b).

2.4. Coronal Heating

2.4.1. Coronal Heating and Magnetic Energy Release

As part of our study of coronal heating, we have performed 3D numerical simulations of the boundary-driven quasi-static magnetic-dissipation model proposed by Parker (1972, 1983) at moderately high values of the Lundquist number *S*. We have concentrated on the dynamics of the electric current and the formation of intense localized current filaments whose dissipation via magnetic reconnection provides an ohmic heating source. We have shown that the coronal plasma response to quasi-static photospheric motions is to produce current filaments via an ideal MHD instability. The line-tied coalescence instability is the most promising model for the observed instability. The detailed results are discussed by Hendrix (1996) and Hendrix & Van Hoven (1997). A detailed description of the reconnection that occurs in the current sheets is described by Schnack, Mikić, & Hendrix (1998).

2.4.2. Coronal Heating by Dissipation of Energy in Coronal Loops

The kink instability of coronal loops plays a fundamental role in the heating of the solar corona. Loops can become linearly unstable, resulting in concentration of the current density in the nonlinear phase of the instability (Einaudi, Lionello, and Velli 1997). The dissipation of these intense current layers is an effective mechanism for converting magnetic energy into thermal energy. We have studied different classes of field models (Velli, Lionello, and Einaudi 1997) using an MHD code in cylindrical coordinates (Lionello, Mikić, & Schnack 1998). The nonlinear evolution of the equilibria shows that loops formed by the slow twisting of magnetic field lines (Mikić, Schnack, & Van Hoven 1990) are more likely to liberate large amounts of energy (Lionello, Velli, Einaudi, & Mikić 1998). The destabilizing role of line-tying in the nonlinear phase of the instabilities has also been addressed (Lionello, Schnack, Einaudi, & Velli 1998).

2.5. Massively Parallel Computing

To improve the efficiency of our computations, and, in particular, to extend our ability to do high-resolution runs, we have investigated how to implement the spherical 3D MHD code on the high performance parallel supercomputers at JPL. The algorithm for the parallel implementation has been designed. A two-dimensional decomposition of the three-dimensional computation domain will be used. Only the (r–θ) plane will be divided among the processing elements (PEs) so that each PE has a range of r and θ, but all ϕ. The Fourier transforms in ϕ can be done without interprocessor communication. At a meeting at SAIC between SAIC, JPL and Caltech researchers, it was decided that, in order to prevent a major code re-write in the future, the code will be re-written in a modern language (High Performance Fortran or Fortran 90) before beginning the parallel implementation. The code will be implemented on the new JPL parallel supercomputer, a Hewlett Packard SPP2000, which uses a PA-8000 chip. The building block of the SPP2000 computer system is a hypernode. Each hypernode is a 16-CPU computer by itself; 4 hypernodes joined together form a supernode. The final configuration for the new machine will be either be a two 128-PE system, or one 256-PE system. The peak speed is 720 Mflops per PE. Sequential code can be run on the machine using global shared memory. At present, the maximum global shared memory is among 64 PEs only. In the future Caltech will help HP to make the global shared memory work on all 256 PEs. The machine supports both Fortran 90 and High Performance Fortran. In order to make our 3D MHD code an efficient parallel code, at present we are leaning to implementing interprocessor communication using a message passing interface (MPI).

3. REFERENCES

Einaudi, G., Lionello, R., & Velli, M. 1997, *Adv. Space Res.*, **19**, 1875.

Habbal, S. R., Esser, R., Guhathakurta, M., & Fisher, R. R. 1995, *Geophys. Res. Lett.*, **22**, 1465.

Hendrix, D. L. 1996, Ph. D. Thesis, University of California, Irvine.

Hendrix, D. L., & Van Hoven, G. 1997, *Ap. J.*, submitted.

Hollweg, J. V. 1978, *Rev. Geophys. Space Phys.*, **16**, 689.

Jacques, S. A. 1977, *Ap. J.*, **215**, 942.

Lee, J., McClymont, A. N., Mikić, Z., White, S. M., & Kundu, M. R. 1998a, *Ap. J.*, **501**, in press.

Lee, J., White, S. M., Kundu, M. R., Mikić, Z., & McClymont, A. N. 1998b, *Solar Phys.*, in press.

Lee, J., White, S. M., Kundu, M. R., Mikić, Z., & McClymont, A. N. 1998c, *Ap. J.*, submitted.

Leka, K. D., Canfield, R. C., McClymont, A. N., & van Driel-Gesztelyi, L. 1996, *Ap. J.*, **462**, 547.

Li, X., Esser, R., & Habbal, S. R. 1997, *J. Geophys. Res.*, **102**, 17419.

Liewer, P. C., Goldstein, B. E., Linker, J. A., Mikić, Z., & Neugebauer, M. 1996, Fall AGU Meeting, San Francisco.

Lionello, R., Linker, J. A., & Mikić, Z. 1998, Spring AGU/SPD Meeting, Boston.

Linker, J. A., & Mikić, Z. 1995, *Ap. J.*, **438**, L45.

Linker, J. A., & Mikić, Z. 1997, in *Coronal Mass Ejections* (N. Crooker, J. Joselyn, and J. Feynman, eds.), *Geophysical Monograph* **99**, American Geophysical Union, p. 269.

Lionello, R., Mikić, Z., & Schnack, D. D. 1998, *J. Comput. Phys.*, **140**, 172.

Lionello, R., Schnack, D. D., Einaudi, G., & Velli, M. 1998, *Phys. Plasmas,* submitted.

Lionello, R., Velli, M., Einaudi, G., & Mikić, Z. 1998, *Ap. J.*, **494**, 840.

Mikić, Z., & Linker, J. A. 1994, *Ap. J.*, **430**, 898.

Mikić, Z., & Linker, J. A. 1996, in *Solar Wind Eight: Proc. of the Eight Intl. Solar Wind Conf.* (D. Winterhalter, J. T. Gosling, S. R. Habbal, W. S. Kurth, and M. Neugebauer, eds.), AIP Conf. Proceedings **382**, AIP Press, Woodbury, N. Y., p. 104.

Mikić, Z., & Linker, J. A. 1997, in *Coronal Mass Ejections* (N. Crooker, J. Joselyn, and J. Feynman, eds.), *Geophysical Monograph* **99**, American Geophysical Union, p. 57.

Mikić, Z., Linker, J. A., & Schnack, D. D. 1996, in *Solar Drivers of Interplanetary and Terrestrial Disturbances* (K. S. Balasubramaniam, S. L. Keil, and R. N. Smartt, eds.), Astron. Soc. Pac., Conf. Series, Vol. **95**, p. 108.

Mikić, Z., & McClymont, A. N. 1994, in *Solar Active Region Evolution: Comparing Models with Observations* (K. S. Balasubramaniam and G. W. Simon, eds), Astron. Soc. Pac., Conf. Series, **68**, 225.

Mikić, Z., Schnack, D. D., & Van Hoven, G. 1990, *Ap. J.*, **361**, 690.

Mok, Y., Van Hoven, G., & Mikić, Z. 1997, *Ap. J.*, **490**, L107.

Neugebauer, M., Forsyth, R. J., Galvin, A. B., Harvey, K. L., Hoeksema, J. T., Lazarus, A. J., Lepping, R. P., Linker, J. A., Mikić, Z., Steinberg, J. T., von Steiger, R., Wang, Y.-M., & Wimmer-Schweingruber, R. 1998, *J. Geophys. Res.*, in press.

Parker, E. N. 1963, *Interplanetary Dynamical Processes* (New York: Wiley-Interscience).

Parker, E. N. 1972, *Ap. J.*, **174**, 499.

Parker, E. N. 1983, *Ap. J.*, **264**, 642.

Rosner, R., Tucker, W. H., & Vaiana, G. S. 1978, *Ap. J.*, **220**, 643.

Schnack, D. D., Mikić, Z., & Hendrix, D. L. 1998, *Ap. J.*, in preparation.

Van Hoven, G., Mok, Y., & Mikić, Z. 1995, *Ap. J.*, **440**, L105.

Velli, M., Lionello, R., & Einaudi, G. 1997, *Solar Phys.*, **172**, 257.

Wang, Y.-M., & Sheeley, N. R., Jr. 1990, *Ap. J.*, **355**, 726.

Withbroe, G. L. 1988, *Ap. J.*, **325**, 442.

4. PUBLICATIONS SUPPORTED BY SPT CONTRACT NAS5-96081 DURING THE FIRST YEAR

1. J. A. Linker and Z. Mikić, "Disruption of a Helmet Streamer by Photospheric Shear", *Ap. J. Lett.* **438**, L45 (1995).
2. Y. Mok and G. Van Hoven, "The Solar-Surface Boundary Conditions of Coronal Magnetic Loops", *Solar Phys.* **161** 67 (1995).
3. G. Van Hoven, D. L. Hendrix, and D. D. Schnack. "The Diagnosis of General Magnetic Reconnection", *J. Geophys. Res.* **100**, 19819 (1995).
4. G. Van Hoven, Y. Mok, and Z. Mikić, "Coronal Loop Formation Resulting from Photospheric Convection," *Astrophys. J. Letters* **440**, L105 (1995).
5. G. Van Hoven, J. A. Linker, and Z. Mikić, "The Evolution, Structure, and Dynamics of the Magnetized Solar Corona," Gather/Scatter (San Diego Supercomputer Center Newsletter), Vol. **11**, No. 3, p. 6, July–September (1995).
6. D. L. Hendrix, "A Study of the Formation and Dissipation of Current Filaments as a Coronal Heating Mechanism," Ph. D. Thesis, University of California, Irvine (1996).
7. D. L. Hendrix, and G. Van Hoven, "Magnetohydrodynamic Turbulence and Implications for Solar Coronal Heating," *Astrophys. J.* **467**, 887 (1996).
8. D. L. Hendrix, G. Van Hoven, Z. Mikić, and D. D. Schnack, "The Viability of Ohmic Dissipation as a Coronal Heating Source," *Astrophys. J.* **470**, 1192 (1996).
9. J. A. Linker, Z. Mikić, and D. D. Schnack, "Global Coronal Modeling and Space Weather Prediction," in *Solar Drivers of Interplanetary and Terrestrial Disturbances* (K. S. Balasubramaniam, S. L. Keil, and R. N. Smartt, eds.), Astronomical Society of the Pacific Conference Series, Vol. **95**, p. 208 (1996).
10. Z. Mikić and J. A. Linker, "The Large-Scale Structure of the Solar Corona and Inner Heliosphere," in *Solar Wind Eight: Proc. of the Eight Intl. Solar Wind Conf.* (D. Winterhalter, J. T. Gosling, S. R. Habbal, W. S. Kurth, and M. Neugebauer, eds.), AIP Conf. Proceedings, **382**, AIP Press, Woodbury, N. Y., p. 104 (1996).
11. Z. Mikić, J. A. Linker, and D. D. Schnack, "Modeling of Active-Region Magnetic Fields," in *Solar Drivers of Interplanetary and Terrestrial Disturbances* (K. S. Balasubramaniam, S. L. Keil, and R. N. Smartt, eds.), Astronomical Society of the Pacific Conference Series Vol. **95**, p. 108 (1996).
12. S. P. Ruden, A. V. R. Schiano, and G. Van Hoven, "A Dynamic Model of the Three-Fluid Solar Wind: Equilibrium Structures and Fluxes," in *Solar Wind Eight: Proc. of the Eight Intl. Solar Wind Conf.* (D. Winterhalter, J. T. Gosling, S. R. Habbal, W. S. Kurth, and M. Neugebauer, eds.), AIP Conf. Proceedings **382**, AIP Press, Woodbury, N. Y., p. 137 (1996).
13. G. Van Hoven, Y. Mok and D. L. Hendrix, "Surface Driven Evolution and Activity of Atmospheric Magnetic Structures" in *Magnetodynamic Phenomena in the Solar Atmosphere*, Kluwer, Dordrecht, p. 51; Proceedings of IAU Colloquium No. 153 (Y. Uchida, T. Kosugi and H.S. Hudson, eds.) (1996).

14. T. Amari, J. J. Aly, J. F. Luciani, T. Boulmezaoud, and Z. Mikić, "Reconstructing The Solar Coronal Magnetic Field as a Force-Free Magnetic Field," *Solar Phys.* **174**, 129 (1997).

15. T. Amari, J. F. Luciani, J. J. Aly, and Z. Mikić, "Opening Solar Magnetic Fields: Some Analytical and Numerical MHD Aspects," in *Coronal Mass Ejections* (N. Crooker, J. Joselyn, and J. Feynman, eds.), Geophysical Monograph **99**, American Geophysical Union, p. 101 (1997).

16. G. Einaudi, R, Lionello, and M. Velli, "Magnetic Reconnection in Solar Coronal Loops," *Adv. Space. Res.* **19**, 1875 (1997).

17. D. L. Hendrix, and G. Van Hoven, "Dynamical Magnetic Reconnection in Parker's Coronal Heating Model," *Adv. Space Res.* **19**, 1865 (1997).

18. L. Jiao, A. N. McClymont, and Z. Mikić, "Reconstruction of the Three-Dimensional Coronal Magnetic Field," *Solar Phys.* **174**, 311 (1997).

19. J. A. Linker and Z. Mikić, "Extending Coronal Models to Earth Orbit," in *Coronal Mass Ejections* (N. Crooker, J. Joselyn, and J. Feynman, eds.), Geophysical Monograph **99**, American Geophysical Union, p. 269 (1997).

20. R. Lionello, "Three Dimensional Imaging for Magnetohydrodynamic Computations," *WSCG'97 Proceedings* (1997).

21. A. N. McClymont, L. Jiao, and Z. Mikić, "Problems and Progress in Computing Three-Dimensional Coronal Active Region Magnetic Fields from Boundary Data," *Solar Phys.* **174**, 191 (1997).

22. Z. Mikić and J. A. Linker, "The Initiation of Coronal Mass Ejections by Magnetic Shear," in *Coronal Mass Ejections* (N. Crooker, J. Joselyn, and J. Feynman, eds.), Geophysical Monograph **99**, American Geophysical Union, p. 57 (1997).

23. Y. Mok, G. Van Hoven, and Z. Mikić, "The Emergence of Current-Carrying Magnetic Loops into the Solar Corona," *Astrophys. J. Letters* **490**, L107 (1997).

24. A. Ruzmaikin, J. D. Anderson, S. Asmar, M. Bird, A. Cacciani, W. Coles, J. Feynman, J. Harvey, K. Harvey, J. Hollweg, J. Linker, Z. Mikić, M. Patzold, and E. J. Smith, "A Spacecraft Going Behind the Sun will Support SOHO," in *The Corona and Solar Wind near Minimum Acttivity* (Proceedings of the Fifth SOHO Workshop), ESA SP-404, 653 (1997).

25. M. Velli, R. Lionello, and G. Einaudi, "Kink Modes and Current Sheets in Coronal Loops," *Solar Physics* **172**, 257 (1997).

26. D. L. Hendrix, and G. Van Hoven, "Fast Magnetic Reconnection and its Role in Coronal Heating," *Ap. J.*, submitted (1997).

APPENDIX

SELECTED REPRINTS

THE ASTROPHYSICAL JOURNAL, 490:L107–L110, 1997 November 20

THE EMERGENCE OF CURRENT-CARRYING MAGNETIC LOOPS INTO THE SOLAR CORONA

Y. MOK AND G. VAN HOVEN
University of California, Irvine, CA 92697
AND
Z. MIKIĆ
Science Applications International Corporation, San Diego
Received 1997 June 24; accepted 1997 September 16; published 1997 October 21

ABSTRACT

The mechanism of the dynamic emergence of current-carrying magnetic loops into the corona is examined by three-dimensional MHD simulations. By simultaneously modeling the spacetime profiles of the normal components of the emerging magnetic field and current density on the photosphere, we demonstrate that this process can qualitatively reproduce observations that show the emergence of a helically twisted magnetic structure with a suitable field-current combination. The flux-tube structure rises into the initially nearly field-free corona and gradually relaxes into a nearly force-free, steady state, magnetic loop.

Subject headings: magnetic fields — MHD — plasmas — Sun: corona — Sun: magnetic fields

1. INTRODUCTION

Coronal loops in the solar atmosphere have been widely observed since the *Skylab* era (Foukal 1976; Krieger 1978; Van Hoven 1981). Their interpretation as plasma loops collimated by active region magnetic fields was later reinforced by *Yohkoh* observations (Klimchuk et al. 1992). Because of their long duration in the solar atmosphere, they are believed to be in stable equilibrium with their environment. Consequently, numerous investigations (using a cylindrical model) have been devoted to studying their physical properties, such as their internal geometry, force balance, and magnetohydrodynamic stability (Raadu 1972; Giachetti et al. 1977; Hood & Priest 1979; Einaudi & Van Hoven 1983; Mikić, Schnack, & Van Hoven 1980).

However, there have been few studies of how these magnetic loops, which carry electric current through the corona, come into existence or of the effects of their quasi-toroidal geometry. In a previous investigation, we addressed some of these issues and reported that these loops can be formed in one way by photospheric plasma vortex motions driven by *high-β* (ratio of fluid to magnetic forces) solar-surface convection (Van Hoven, Mok, & Mikić 1995). Vortical motions at the poles twist the in situ bipolar field lines at the base and induce an azimuthal field component into the field structure as well as a toroidal current along the to-be-formed loop.

However, recent observations also support a second scenario in which magnetic flux already carries electric current at the time of emergence into the corona (Leka et al. 1996). The physical process of emerging current-carrying flux into a nearly field-free corona is fundamentally different from twisting existing field lines. While the latter does not change the *total* flux at the base, the former injects new flux through the base. How the plasma-field in the corona responses to this injection is reported in this Letter. To simulate the observation, we use a numerical model to describe the *dynamic* formation of magnetic loops within the framework of three-dimensional MHD. The results provide the first realization of the simultaneous emergence of toroidal fields *and* currents, in contrast to the work of McClymont & Mikić (1994) in which only current was injected. We succeed in representing one physical mechanism for the often observed emergence of flux into the solar corona.

2. PHYSICAL AND COMPUTATIONAL MODELS

We model this type of flux emergence by starting with a small background magnetic field embedded in the coronal plasma. Magnetic field and current density are then injected into a Cartesian computational domain at the base. It is argued that magnetic flux, coexisting with axial current density, is in the form of a flux rope created below the surface in a high-β plasma. As buoyancy brings the loop to the surface, the combined, self-consistent, field/current simply appears on the photosphere. From a computational point of view, we are treating this process as a phenomenological problem. That is, we are interested in understanding how the field/current develops *in the corona* as a response to the evolving conditions on the photospheric surface. The physical process under the surface is not fully understood (Fan, Fisher, & McClymont 1994; Longcope, Fisher, & Arendt 1996) and is not part of our computational domain.

Our approach in this work is justified because the photosphere is a high-β plasma, which can control how the flux should emerge, and is a boundary of the computational domain, which is strictly regarded as the low-β corona. We merely model the magnetic field and the current density at this boundary, according to observations, to provide a driving term in the dynamic equations. To do this, we specify the normal components of the magnetic field and the current density at this surface to simulate those of the emerging flux rope. Further specification on the boundary, such as the tangential components of either quantity, will result in overspecification and inconsistency in our algorithm.

We describe the coronal dynamics with a reduced set of the full MHD equations. The main nonstandard assumption used is that of constant density and pressure as justified (partially a posteriori) by Ortolani & Schnack (1993) for nearly force-free fields in the absence of significant energy transport. The physical motivation behind this assumption is that the corona is a low-β plasma and thus density-variation and plasma-pressure effects are most likely negligible in the presence of the dom-

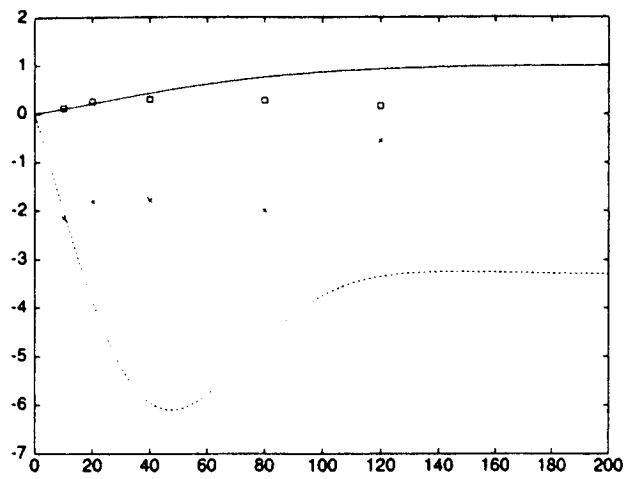

FIG. 1.—Time profiles of the emerging B_{0z} and J_{0z} at the center of the poles at the base, along with five actual peak values of B_z and J_z at the *apex*.

inant magnetic forces. Under these *approximations*, we are left with a system governed by two coupled differential equations describing magnetic induction and fluid momentum transport:

$$\partial \boldsymbol{A}/\partial t = \boldsymbol{v} \times \boldsymbol{B} - \eta \boldsymbol{J}, \tag{1}$$

$$\rho(\partial \boldsymbol{v}/\partial t + \boldsymbol{v} \cdot \nabla \boldsymbol{v}) = \boldsymbol{J} \times \boldsymbol{B} + \nu\rho\nabla^2 \boldsymbol{v}, \tag{2}$$

where $\boldsymbol{A}$ is the vector potential, $\boldsymbol{v}$ is the plasma flow velocity (maintained below 3% of the Alfvén speed throughout the evolution), ρ is the plasma density, η and ν are the resistivity and viscosity, respectively, written in the customary dimensionless units of MHD (Ortolani & Schnack 1993). The magnetic field $\boldsymbol{B}$ and current density $\boldsymbol{J}$ are given by

$$\boldsymbol{B} = \nabla \times \boldsymbol{A} \quad \text{and} \quad \boldsymbol{J} = \nabla \times \boldsymbol{B}. \tag{3}$$

The implementation of the emerging magnetic field and current density begins with a pair of predefined spacetime profiles for B_{0z} and J_{0z}, specified only at the base. Since the vector potential $\boldsymbol{A}$ is the actual dynamic variable, with $\boldsymbol{B}$ and $\boldsymbol{J}$ being postcomputed quantities, the desired values of B_z and J_z at the boundary, i.e., B_{0z} and J_{0z}, must be integrated to obtain the corresponding evolving value of $\boldsymbol{A}$. Because of the staggered grids used for $\boldsymbol{A}$ in the finite-differencing scheme, only its tangential components $\boldsymbol{A}_t$ are imposed as a time-varying boundary condition. To advance $\boldsymbol{A}_t$ at the base, we first evaluate the tangential electric field $\boldsymbol{E}_t$ contributed by B_{0z} and J_{0z}. In general, $\boldsymbol{E}_t$ can be expressed as $\nabla_t \times \hat{z}\psi - \nabla_t\phi$, where the first part is induced by the emerging B_{0z} and the second is determined by J_{0z}. The induced part ψ can be obtained by solving the equation

$$\nabla_t^2 \psi = \partial B_{0z}/\partial t. \tag{4}$$

To achieve the desired current density J_{0z} at the base, an electric potential ϕ is also applied at the boundary. The purpose is to create a potential difference between the two ends of each field line in order to drive a current. Effectively, each field line through the corona is a circuit with an equivalent battery connecting its two ends beneath the surface. Since we are only modeling the intended electric current J_{0z} phenomenologically, we are not concerned with the actual mechanism below the surface that drives this current. In order to make the actual computed J_z approach the desired J_{0z}, ϕ is chosen to satisfy the equation

$$\partial\phi/\partial t = (J_{0z} - J_z)/\tau_c, \tag{5}$$

where τ_c is a time constant, chosen to be ~0.1 of the rise time of the emerging B_z, so that the current will closely follow the field. This source-term algorithm has also been used by McClymont & Mikić (1994; McClymont, Jiao, & Mikić 1997) in the presence of fixed B_{0z} sources.

Finally, the tangential vector potential $\boldsymbol{A}_t$ at the base evolves in time according to Maxwell's equation

$$\partial \boldsymbol{A}_t/\partial t = -\boldsymbol{E}_t. \tag{6}$$

With this time-dependent boundary condition for $\boldsymbol{A}_t$ at the base, equation (1) is advanced with additional conditions on the other five surfaces where $\boldsymbol{B}_n$ and $\boldsymbol{E}_t$ vanish. The momentum equation (2) is advanced with the *base* boundary condition that Ohm's law is satisfied,

$$\boldsymbol{v} = \boldsymbol{E} \times \boldsymbol{B}/\boldsymbol{B}^2, \tag{7}$$

and $\boldsymbol{v} = 0$ on the other five surfaces.

The magnetic loop is taken to lie eventually along the x-axis with footpoints at $x = \pm 1$. We choose the dimensionless size of the rectangular domain to be $12 \times 12 \times 8$, a box sufficiently large compared to the magnetic structure to avoid boundary effects. A variable-size mesh of $127 \times 83 \times 67$ is used. Before the emergence of the loop, the initial state consists of a small background field as is commonly seen in the solar atmosphere. We simulate this background with a simple potential field, specified by its normal component at the base to be $\tanh(x/L)$ with a magnitude of 5% of the expected strength of the loop field. The spacetime profiles of the emerging magnetic field and current density are chosen as follows. The two magnetic poles, located at the base boundary with opposite polarities, are given by $B_{0z}(x, y, t; R) = +f_B(t)\exp(-[(x - x_R)^2 + y^2]/a^2)$ for the right pole and similarly, with opposite sign, for the left. Here $f_B(t)$ is the time profile of the emerging field, and $(x_R(t), 0)$ and $(x_L(t), 0)$ are the coordinates of the centers of the poles. They are initially located at $x_{R,L} = \pm 0.2$ at the beginning and move to the final locations at $x_{R,L} = \pm 1.0$ with the same time profile. The Gaussian width of the profile is chosen to be $a = 0.5$. The peak value of $B_{0z,R}$ is shown in Figure 1.

The current density also consists of two opposite poles with their centers coinciding with the magnetic poles at all time. The spatial profile is chosen in such a way that the integrated net current for each pole is zero. Although this condition is not necessary, it is convenient for computational purposes and can easily be relaxed to consider a more general case in which a reverse-current layer would be self-induced (Van Hoven et al. 1995). The profile for the right pole, for example, is $J_{0z}(x, y, t; R) = \alpha f_J(t)\,(1 - r_R^2/c^2)\exp(-r_R^2/b^2)B_{0z}(x, y, t, R)$, where $f_J(t)$ is the model time profile, $r_R^2 = (x - x_R)^2 + y^2$, and $c^{-2} = a^{-2} + b^{-2}$. The width of the current profile is chosen to be $b = 0.6a$. The parameter α (taken to be negative) is the

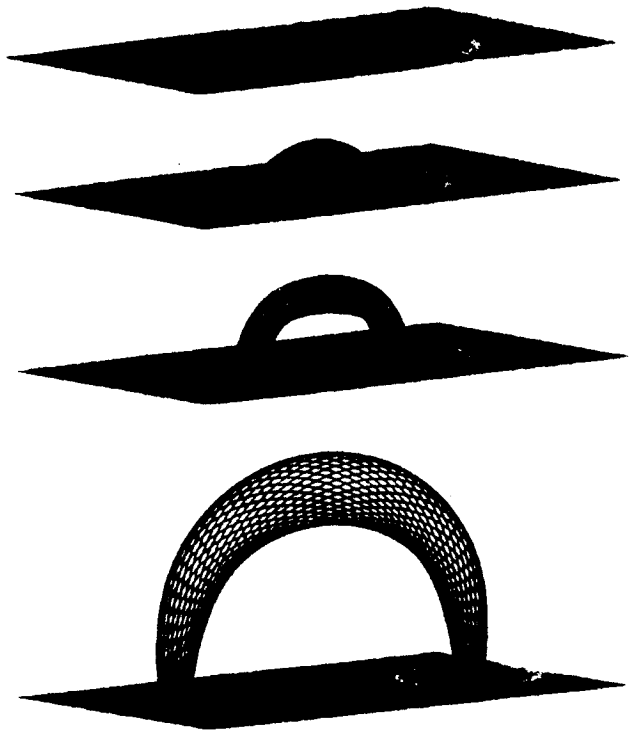

FIG. 2.—Field lines in the loop region (*see text*) at times (*top to bottom*) t = 10, 20, 40, and 360.

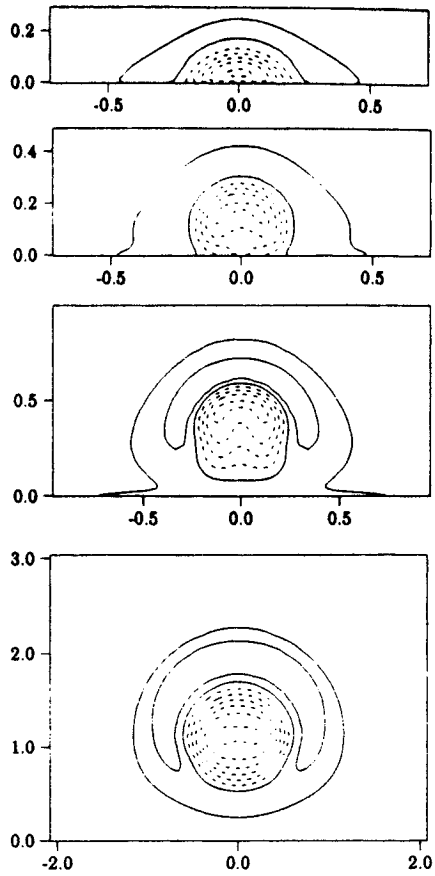

FIG. 3.—(*Top*) Contours of α^* at the midplane (x = 0) at time t = 10. Only the central section, where magnetic flux is emerging, is plotted. The entire domain is $-6 < x, y < 6$, $0 < z < 8$. The base plane limits are $\alpha^*(\min) = -10.1$ and $\alpha^*(\max) = 1.5$. Dashed lines indicate that the contour values are negative. The emerging flux does not yet have the appearance of a loop. Notice that the scales of each panel are all different to make the illustration more legible. (*Second from top*) Contours of α^* at t = 20. $\alpha^*(\min) = -7.5$ and $\alpha^*(\max) = 2.5$. The flux tube begins to rise from the surface. (*Third from top*) Contours of α^* at t = 40. $\alpha^*(\min) = -7.4$ and $\alpha^*(\max) = 2.1$. The loop has levitated from the surface. (*Bottom*) Contours of α^* at t = 360. $\alpha^*(\min) = -1.8$ and $\alpha^*(\max) = 0.9$. The loop has relaxed to its equilibrium state.

nominal ratio of J/B in a force-free field. (The use of α is conventional but does not indicate that the independently emerging values of $\boldsymbol{B}$ and $\boldsymbol{J}$ are anywhere near force-free.) The peak current density at the center of the right pole is also shown in Figure 1. The profile of the left pole is chosen in a similar manner. The purpose of specifying the poles in this way is to model the normal components of the flux rope as it surfaces dynamically through a quiet photosphere. The value of α, chosen to be -3.3, is the intended limiting value of the force-free parameter, evaluated at the pole center, as the loop relaxes to the time-asymptotic, equilibrium, force-free state. In the simulation described below, the rise time of the magnetic field is set to 100 Alfvén transit periods, which is approximately 10–20 minutes for typical coronal parameters.

3. RESULTS

As the subphotospherically generated values of $\boldsymbol{B}$ and $\boldsymbol{J}$ emerge, they are far from force-free, as they must be in the low-β corona. Thus, the fields dynamically evolve, by rising and expanding, in moving toward this state. In the following, we provide the first description of the details of this oft-imagined process.

Figure 2 (*top*) shows the magnetic field lines at time t = 10. The magnetic structure has just emerged from the surface and is still close to the photosphere. It lacks the physical appearance of a "loop" in the conventional sense as we can expect from a low-lying structure. The loop is characterized by the torsion parameter $\alpha^*(\boldsymbol{r}; t) = \boldsymbol{J} \cdot \boldsymbol{B}/B^2$, which generally describes the local behavior of the field lines in a sheared field. The contours of $\alpha^*(y, z; t = 10)$ at the midplane (x = 0) are shown in Figure 3 (*top*). The local maximum of $|\alpha^*|$ can be considered to be the loop "axis," connecting the two poles on the surface. The value of α^* near the axis is negative because the local $\boldsymbol{J}$ and $\boldsymbol{B}$ have been chosen to be in opposite directions; $\alpha^*(\boldsymbol{r}; t)$ increases away from this axis, then changes sign at some distance from the axis, before eventually going to zero. The "apex" of the loop axis is at an altitude of only 0.035. Field lines are drawn around this axis to depict the nature of the magnetic structure. The moderate pitch angle of the helical field lines clearly shows the effect of current flowing along the loop axis.

Note that the system is far from being force-free at this early time. In fact, the loop is dynamically rising and toroidally expanding as driven by the increasing $\boldsymbol{J} \times \boldsymbol{B}$ force. Hence, $\alpha^*(\boldsymbol{r})$ should not be confused with the conventional α in a force-free field, although the former asymptotically approaches the latter. At the midplane, the absolute value of α^*, which is approximately equal to J_x/B_x locally, is larger than the intended α of the final state. However, the loop is not MHD unstable because the field lines are relatively short, and the most unstable, long-wavelength modes are not accessible to the loop.

The plasma flow at the base has both normal and tangential components. The existence of a finite normal component indicates that there is a net inflow into the box. However, the upward flow is confined mostly to a neighborhood directly under the apex with a maximum velocity less than $0.02v_A$.

Figure 2 (*second from top*) shows the magnetic field lines at $t = 20$. The magnetic structure has taken on the characteristic low-lying loop shape. The corresponding contours of $\alpha^*(y, z)$ are shown in the second panel of Figure 3. The contours of the loop part are not circular because the central part is rising into the corona at a speed of $0.023v_A$, somewhat more quickly than either side at $8.3 \times 10^{-3}v_A$. The dynamic nature of the structure at this instant can be seen by reference to Figure 1, showing that both B_{0z} and J_{0z} are in rapidly rising phases. Field lines are drawn around this α^* channel as before. Figure 2 (*third from top*) shows the magnetic field lines at $t = 40$, and the third panel in Figure 3 shows the corresponding contours of α^*. The loop has risen to a substantial altitude so that its bottom side has truly detached from the photosphere. The main current channel, with negative α^*, is surrounded by the return current (positive α^*). The current density is near its peak value in time, and the loop axis is still rising at a speed of $0.022v_A$.

Finally, we advance the equations until $t = 360$, at which time both J_{0z} and B_{0z} have reached their respective asymptotic values. The loop has now relaxed to its equilibrium state. The field lines and α^* are shown in Figures 2 and 3 (*bottom panels*). The altitude of the axis of the loop apex is 1.1, and the radius of the main current channel is approximately 0.5. The structure of the cross section is now qualitatively similar to Figure 4 of Van Hoven et al. (1995). Note that the α contours at the base in this earlier model computation are not circular, but the flow is, by design. In the present case, the α contours at the base are circular by design, while the plasma flow reacts to a magnetic force that is not circular. Hence, these two cases are only qualitatively the same even when we try to set α at the center of the poles to the same value.

Because of the finite resistivity, a small electric potential Φ, though constant in time, is needed at the base to maintain the current. The resulting tangential electric field causes a small plasma vortex around each pole as indicated by $\boldsymbol{E} \times \boldsymbol{B}/B^2$ with a maximum speed of $4 \times 10^{-3}v_A$. In this state, the magnetic loop is only approximately force-free, since the integrated (over the entire box) value of $|\boldsymbol{J} \times \boldsymbol{B}|$ is just under 8% of the integrated $|\boldsymbol{J} \cdot \boldsymbol{B}|$. This is due to the relatively small Lundquist number we use (10^4). The electric potential that keeps the current from decaying due to ohmic dissipation induces an $\boldsymbol{E} \times \boldsymbol{B}$ drift of the plasma. This finite velocity must be balanced by a finite $\boldsymbol{J} \times \boldsymbol{B}$ force in equation (2) to maintain a steady state. In reality, the Lundquist number in the corona is $\sim 10^{12}$, and the loop is closer to being force-free than the computational results indicate.

4. SUMMARY AND DISCUSSION

We have described the first demonstration of the dynamic *emergence* of a magnetic loop structure from the solar surface. We have taken a phenomenological approach by modeling the observed growth of the line-of-sight magnetic field and current density on the photosphere, in addition to making a number of well-accepted theoretical assumptions.

As the emerging field and current density at the base reach their predetermined values, the magnetic loop gradually settles into a nearly force-free equilibrium as the kinetic energy of the plasma motions and the integrated magnetic force decay to vanishingly small values. The internal structure of the loop, including the field geometry and the current distribution, is qualitatively similar to the magnetic loop exhibited in our previous work (Van Hoven et al. 1995), although the loop is formed through an entirely different, observationally motivated, process and driven by a different mechanism. Finally, we want to point out that we have chosen a specific set of parameters in this simulation. For example, the time profile of the current density is carefully chosen so that the emerging magnetic-field lines display visible twists as in observations, and yet the loop does not cross the ideal-MHD stability boundary (Van Hoven 1981). There are many physically acceptable regions in the parameter space that we have not explored. In addition, there is always the question of possible ideal MHD or resistive instability, or flaring, when the loop is overdriven. We plan to investigate these issues in future studies.

The authors acknowledge helpful discussions with Dalton Schnack and Jon Linker. This research was supported, in part, by the SPT program of NASA and the ATM section of NSF. Computational services were provided by UCI and NSF at SDSC, and DOE at NERSC.

REFERENCES

Einaudi, G., & Van Hoven, G. 1983, Sol. Phys., 54, 107
Fan, Y., Fisher, G. H., & McClymont, A. N. 1994, ApJ, 436, 907
Foukal, P. V. 1976, ApJ, 210, 575
Giachetti, R., Van Hoven, G., & Chiuderi, C. 1977, Sol. Phys., 55, 371
Hood, A. W., & Priest, E. R. 1979, Sol. Phys., 64, 303
Klimchuk, J. A., Lemen, J. R., Feldman, U., Tsuneta, S., & Uchida, Y. 1992, PASJ, 44, L181
Krieger, A. S. 1978, Sol. Phys., 56, 107
Leka, K. D., Canfield, R. C., McClymont, A. N., & van Driel-Gesztelyi, L. 1996, ApJ, 462, 547
Longcope, D. W., Fisher, G. H., & Arendt, S. 1996, ApJ, 464, 999
McClymont, A. N., Jiao, L., & Mikić, Z. 1997, Sol. Phys., in press
McClymont, A. N., & Mikić, Z. 1994, ApJ, 422, 899
Mikić, Z., Schnack, D. D., & Van Hoven, G. 1990, ApJ, 361, 690
Ortolani, S., & Schnack, D. D. 1993, Magnetohydrodynamics of Plasma Relaxation (Singapore: World Scientific), 42
Raadu, M. A. 1972, Sol. Phys., 22, 425
Van Hoven, G. 1981, in Solar Flare Magnetohydrodynamics, ed. E. R. Priest (New York: Gordon & Breach), pp. 217–275
Van Hoven, G., Mok, Y., & Mikić, Z. 1995, ApJ, 440, L105

The Initiation of Coronal Mass Ejections by Magnetic Shear

Zoran Mikić and Jon A. Linker

Science Applications International Corporation, San Diego, California

Theoretical MHD models have shown that magnetic shear, which can be induced in coronal magnetic fields by photospheric flows (including differential solar rotation), can lead to the destabilization of large-scale coronal magnetic arcades and coronal streamers. When the shear exceeds a critical threshold, helmet streamers erupt, with characteristics that are generally similar to observations of coronal mass ejections (CMEs). These results indicate that magnetic shear can be considered to be a candidate for the initiation of CMEs. We discuss the concept of magnetic shear in the corona, and we describe its role in the energization of the coronal magnetic field. We review some theoretical results on the shearing of axisymmetric coronal arcades and streamers, and we present preliminary results on the evolution of a three-dimensional model of the solar corona at solar minimum, including the eruption of magnetic fields that resemble a CME.

1. INTRODUCTION

Although CMEs have now been observed for over two decades, we still do not known how they are initiated. The principal reason for this lack of understanding is that CMEs have been observed on the solar limb, where it is difficult to correlate them with changes in the photospheric magnetic field. Since the coronal magnetic field cannot be measured in general, the magnetic structure of coronal streamers prior to, and during eruption, is not known. Two promising developments in observations of CME initiation have occurred recently. First, a significant correlation has been shown to exist between erupting filaments observed on the solar disk and emergence of new flux [*Feynman and Martin*, 1995], which implies that emerging flux may initiate CMEs, since CMEs frequently (but not always) contain an erupting filament. Second, interpretations of Yohkoh SXT observations have shown that CMEs may be associated with "dimming" of the X-ray corona [e.g., *Hudson et al.*, 1996]. These observational techniques can relate CMEs to conditions in the photosphere and corona, and may help to identify the mechanism of CME initiation.

In order to develop a complete understanding of CMEs, a corresponding *theoretical* study of CME initiation is required. Since a CME expels a large amount of mass (up to 10^{16} g) into the solar wind and liberates a substantial amount of thermal energy in the corona, a successful theoretical model must demonstrate how this energy can be stored in the corona prior to eruption, in addition to showing how this energy can be released impulsively.

Over the last several years, theoretical models of the large-scale corona have evolved considerably. Simple idealized models have given way to sophisticated models which, in the near future, will allow us to follow the three-dimensional evolution and eruption of coronal streamers that match measured photospheric magnetic fields. Such models are useful for developing intuition about the properties of coronal streamers, testing hypotheses about CME initiation mechanisms, understanding the signatures of interplanetary CME observations, and eventually, being able to forecast the trajectory of CMEs, a principal goal of the National Space Weather Program.

In this paper we describe the use of theoretical models to study the role of magnetic shear in the initiation of CMEs.

Coronal Mass Ejections
Geophysical Monograph 99

Our results indicate that, from a theoretical point of view, an increase of magnetic shear may be the mechanism by which coronal mass ejections are initiated. The role of magnetic shear will undoubtedly be clarified in the future by more realistic theoretical calculations and with better observations of CMEs.

2. MAGNETIC SHEAR

The magnetic field is the principal mechanism by which energy can be stored in the lower solar corona. The term "magnetic shear" has been used loosely to refer to the energized state of the magnetic field in the solar corona. To illustrate the definition of magnetic shear, consider the idealized situation of a force-free field [e.g., *Priest*, 1982, p. 119], a good approximation to the state of strong magnetic fields in active regions, in which magnetic forces dominate other forces. In this approximation, the magnetic field is the only source of energy. The potential magnetic field is the lowest energy state for a given flux distribution in the photosphere. Therefore, in order to release energy, the magnetic field needs to be "energized" above the potential state. The magnetic field can be energized by being twisted; the electric currents associated with this twist provide a source of free energy that can, in principle, be released during an eruption. (Within the force-free model, the electric currents associated with this twist would flow along the magnetic field.) One way in which the coronal magnetic field can be twisted is by (non-uniform) photospheric flows. Convective flows in the dense photosphere tend to move the footpoints of the magnetic field lines that penetrate it through the effect of line tying [e.g., *Raadu*, 1972; *Einaudi and Van Hoven*, 1981; *Priest*, 1982]. We refer to the twist introduced by this effect as *photospheric shearing*. Magnetic twist can also arise in the corona from the eruption of twisted (current-carrying) fields from below the photosphere [e.g., *Leka*, 1995; *Lites et al.*, 1995]. The twist that energizes the magnetic field above the potential state has been termed *magnetic shear*. Note that magnetic shear includes twisting by photospheric shear flows as well as the twist introduced by eruption of twisted magnetic flux from below the photosphere.

In the context of coronal mass ejections, the situation is more complicated than in the idealized case of force-free magnetic fields, since additional sources of energy, including the kinetic energy in the flowing solar wind, gravitational potential energy, and thermal plasma energy, become important. Nevertheless, the concept of magnetic shear can still be used to express the energization of the coronal magnetic field.

In this paper we discuss magnetic shear introduced by the effect of photospheric flows only. The important effect of increasing magnetic shear through emerging flux is not addressed here. We describe how photospheric shear can store energy in the coronal magnetic field, and how it can lead to eruption. Such photospheric flows can arise from differential rotation and other large-scale flows in the photosphere. We therefore refer to the "shearing" of the large-scale coronal field by photospheric flows.

Magnetic field observations that are readily available today (e.g., synoptic maps of the normal component of the magnetic field in the photosphere deduced from line-of-sight magnetograms, from Wilcox Solar Observatory and the National Solar Observatory at Kitt Peak) cannot specify the magnetic shear in the corona. In order to fully specify the state of the corona, and in particular, its level of energization, it is necessary to specify the transverse component of the magnetic field. Thus, a fundamental aspect of the state of solar magnetic field is not provided by these magnetograms, as they do not allow configurations with different levels of magnetic shear to be distinguished. As is well known from studies of magnetic fields in active regions, a *vector* magnetogram is required to uniquely specify the magnetic field [*Mikić and McClymont*, 1994; *Mikić et al.*, 1996]. In principle, full-disk vector magnetograms can provide information about the transverse component of the magnetic field. Whether this can be done with sufficient accuracy to determine the relatively weak large-scale field is not known at present. In the future, the development of this capability will improve our ability to model and assess the state of magnetic shear in the solar corona.

Let us illustrate this situation by means of an idealized example. Consider the case of an axisymmetric equilibrium. The equilibrium magnetic field in the corona for a given normal magnetic field distribution in the photosphere (e.g., that corresponding to a dipole) can be found by solving the steady-state MHD equations with finite resistivity. We normally find the steady-state solution using a relaxation scheme, by integrating the time-dependent MHD equations to steady state with a fixed normal component of the magnetic field in the photosphere. The resulting solution is a "minimum magnetic shear" solution (loosely speaking) for the given boundary conditions, since it is found by a relaxation procedure in the presence of plasma resistivity. It will be the solution with the smallest twist in the magnetic field compatible with the specified normal magnetic field. The solution consists of the canonical coronal streamer configuration described by Pneuman and Kopp [1971], containing a dense closed-field region, in which the solar wind flow is arrested, surrounded by open magnetic field lines along which the solar wind flow streams to supersonic velocities. The magnetic field is potential (current-free) nearly everywhere, except in a narrow layer surrounding the open-closed field boundary, and along a sheet that extends from the tip of the coronal streamer to infinity, at which the current is concentrated into a sheet. Figure 1 shows an example of a configuration we computed with a dipole magnetic flux distribution [*Linker and Mikić*, 1995]. The current sheet that borders the open/closed field

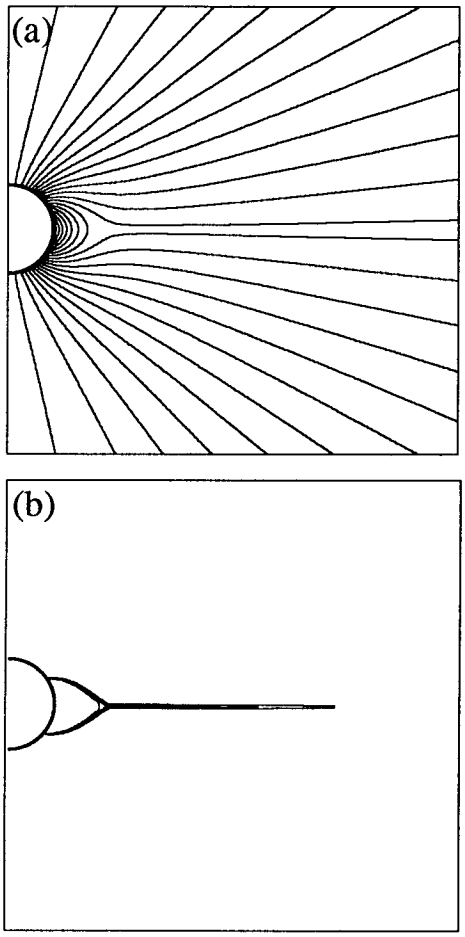

Figure 1. (a) Magnetic field lines (contours of constant flux ψ), and (b) contours of the azimuthal current density (J_ϕ) in an axisymmetric helmet streamer. A current sheet separates fields of opposite polarity and bounds the closed field region; away form the current sheet the field is nearly potential. The solar wind plasma flows outward along field lines in the open-field region, but is essentially stationary inside the closed-field region.

boundary is caused by the discontinuity of the magnetic field pressure, which in turn is induced by the discontinuity in plasma pressure between the open and closed field regions.

In this idealized axisymmetric case, the field lines have an arcade-like geometry in the closed-field region, where the field is entirely poloidal, with zero azimuthal (B_ϕ) magnetic field. In addition, the parallel component of the electric current density is everywhere zero. It is this component that is associated with the twist in the magnetic field. Therefore, this state is not likely to represent the state of the corona at any time, since it corresponds to a magnetic field that has no twist in it. This field is not likely to erupt without additional energization.

This equilibrium can be energized by twisting the magnetic field. In general, photospheric flows will twist the magnetic field, introducing magnetic shear. As noted above, without detailed observations of the transverse magnetic field it is not possible to uniquely determine the magnetic shear in the coronal field, so that at present we are limited to using phenomenological photospheric shear flow profiles to increase the twist of the magnetic field to a level that will cause eruption.

Therefore, the magnetic shear in our "initial" equilibrium state is not likely to correspond to that of the corona at any time, but is merely a starting point for our computations. In particular, this is the reason that a significant amount of shear is needed to cause the first eruption in our simulations (described below), since we start with a state which has minimum magnetic shear. Subsequent eruptions do not require as much shear. In principle, once vector magnetic field measurements become available, it may be possible to construct a coronal magnetic field equilibrium with a level of magnetic shear that corresponds to the state of the corona corresponding to the particular time of the magnetic field observation. At present, lacking more complete observational information about the state of the magnetic field, our best alternative is to energize the field (by applying phenomenological photospheric flows) to a level of magnetic shear that causes eruption to occur.

3. AN MHD MODEL OF THE SOLAR CORONA

A self-consistent description of the large-scale solar corona requires the coupled interaction of magnetic, plasma, and solar gravity forces, including the effect of the solar wind. In the magnetohydrodynamic (MHD) model, the coronal plasma is described by the following equations:

$$\nabla \times \mathbf{B} = \frac{4\pi}{c}\mathbf{J} , \tag{1}$$

$$\nabla \times \mathbf{E} = -\frac{1}{c}\frac{\partial \mathbf{B}}{\partial t} , \tag{2}$$

$$\mathbf{E} + \frac{1}{c}\mathbf{v} \times \mathbf{B} = \eta \mathbf{J} , \tag{3}$$

$$\frac{\partial \rho}{\partial t} + \nabla\cdot(\rho \mathbf{v}) = 0 , \tag{4}$$

$$\rho\left(\frac{\partial \mathbf{v}}{\partial t} + \mathbf{v}\cdot\nabla\mathbf{v}\right) = \frac{1}{c}\mathbf{J} \times \mathbf{B} - \nabla p - \nabla p_w + \rho \mathbf{g} + \nabla\cdot(\nu\rho\nabla\mathbf{v}) , \tag{5}$$

$$\frac{\partial p}{\partial t} + \nabla\cdot(p\mathbf{v}) = (\gamma - 1)(-p\nabla\cdot\mathbf{v} + S) , \tag{6}$$

where $\mathbf{B}$ is the magnetic field intensity, $\mathbf{J}$ is the electric current density, $\mathbf{E}$ is the electric field, $\mathbf{v}$, p, and ρ are the plasma velocity, pressure, and mass density, $\mathbf{g}$ is the gravitational acceleration, η is the plasma resistivity, ν is the kinematic plasma viscosity, S represents energy source

terms, and the wave pressure p_W represents the acceleration due to Alfvén waves.

The application of this model to the structure and dynamics of the solar corona and inner heliosphere is discussed by Linker and Mikić [1997, in this volume]. Our thermodynamic model is presently being improved by including the effects of coronal heating, parallel thermal conduction, radiation loss, and acceleration due to Alfvén waves. We do not consider these improvements here. In the present application, we use the polytropic model [*Parker*, 1963] with an adiabatic energy equation ($S = 0$) with $\gamma = 1.05$, and no Alfvén waves ($p_W = 0$).

We have developed a three-dimensional code to solve equations (1)–(6) in spherical coordinates, as described by Mikić and Linker [1994]. This time-dependent model has been used to study the evolution of axisymmetric magnetic arcades [*Mikić and Linker*, 1994] and helmet streamers [*Linker and Mikić*, 1995], as well as the three-dimensional structure of the corona [*Mikić and Linker*, 1996; *Linker et al.*, 1996; *Linker and Mikić*, 1997].

4. DISRUPTION OF AXISYMMETRIC CORONAL ARCADES AND STREAMERS

Our efforts to understand CMEs have focused on first distilling the essential physics from the simplest model possible (disruption of axisymmetric coronal magnetic arcades), and then incorporating these effects into more realistic models of the solar corona (including the effect of the solar wind, differential rotation, and three-dimensional geometry).

The properties and stability of coronal magnetic fields have been studied extensively [see the references in *Mikić and Linker*, 1994]. In order to study the theoretical aspects of CME initiation, we started with the simplest model possible: we assumed zero beta [i.e., magnetic forces dominate plasma forces, so that we can neglect ∇p in Eq. (5)], a fixed density, we neglected gravity, and we modeled two-dimensional (axisymmetric) variation. We investigated the dynamical evolution of an initially dipolar magnetic field arcade subjected to idealized photospheric shearing motions [*Mikić and Linker*, 1994]. The calculations were performed using both the ideal and resistive MHD equations. When an arcade is subjected to a photospheric shear flow profile, the arcade evolves quasi-statically for small amounts of shear. During this phase, poloidal magnetic field (B_r, B_θ) is converted into azimuthal magnetic field (B_ϕ), and the magnetic energy increases with increasing magnetic shear as the field becomes more and more twisted; energy is therefore stored in the magnetic field. However, when a critical shear is exceeded, the field expands rapidly and produces a concentration of the electric current density. An ideal MHD (i.e., zero resistivity) calculation shows that a transition to a partially open configuration occurs at the critical shear value. In this state a small fraction of the magnetic field lines are closed but the majority of field lines (97% of the flux) are open. The open field lines of opposite polarity are separated by a tangential discontinuity. The magnetic energy of this partially open configuration is close to but less than the energy in a fully open field [*Aly*, 1984, 1991; *Sturrock*, 1991].

The transition to a partially open field requires an initially smooth magnetic field to evolve into one with discontinuities; this process has been described as magnetic nonequilibrium [*Parker*, 1972, 1979; *Priest*, 1981; *Vainshtein and Parker*, 1986]. The appearance of a discontinuity implies that even a small amount of plasma resistivity is important. When we included finite resistivity, the discontinuity was resolved into a current sheet which was subsequently the site of rapid magnetic reconnection, leading to fast flows and the ejection of a plasmoid [*Mikić and Linker*, 1994]. These results suggest that CMEs may be initiated by the destabilization of magnetic arcades by photospheric shear. The rapid inflation of the field at the critical shear value was also found by Roumeliotis *et al.* [1994].

Having found the underlying cause of the disruption of magnetic configurations, we applied our model to a more realistic equilibrium. A comparison with CME observations requires the important effect of the solar wind to be included. We started with an axisymmetric helmet streamer equilibrium corresponding to a dipole magnetic field distribution at the solar surface [*Pneuman and Kopp*, 1971], which was developed by integrating the time-dependent resistive MHD equations to steady state [*Steinolfson et al.*, 1982; *Linker et al.*, 1990; *Wang et al.*, 1993]. The evolution of this field in response to photospheric shear flow is qualitatively similar to that of the arcade. The closed-field region initially expands slowly as the field evolves quasi-statically; when a critical shear is reached, the magnetic field lines erupt outward, driving plasma into the outer corona. While the underlying reason for the disruption is the same in both cases (ideal MHD magnetic nonequilibrium), once the streamer begins to rise, the plasma within it accelerates into the solar wind, stretching and opening the magnetic field lines, and creating a current sheet at which the low-lying loops subsequently reconnect [*Linker and Mikić*, 1995]. As the reconnection proceeds, the closed-field region grows in size as successively higher loops reconnect [*Kopp and Pneuman*, 1976], a phenomenon that has been observed in Yohkoh soft X-ray images [*Hiei et al.*, 1993; *Tsuneta*, 1996].

These studies of arcades and helmet streamers used idealized photospheric flow profiles to induce the magnetic shear. One component of photospheric motions that may contribute to the energization of large-scale coronal fields is differential rotation. We have investigated how differential rotation [*Snodgrass*, 1983] affects axisymmetric coronal streamers over many rotations. As in the case of the idealized shear profile, the streamer disrupts when a critical

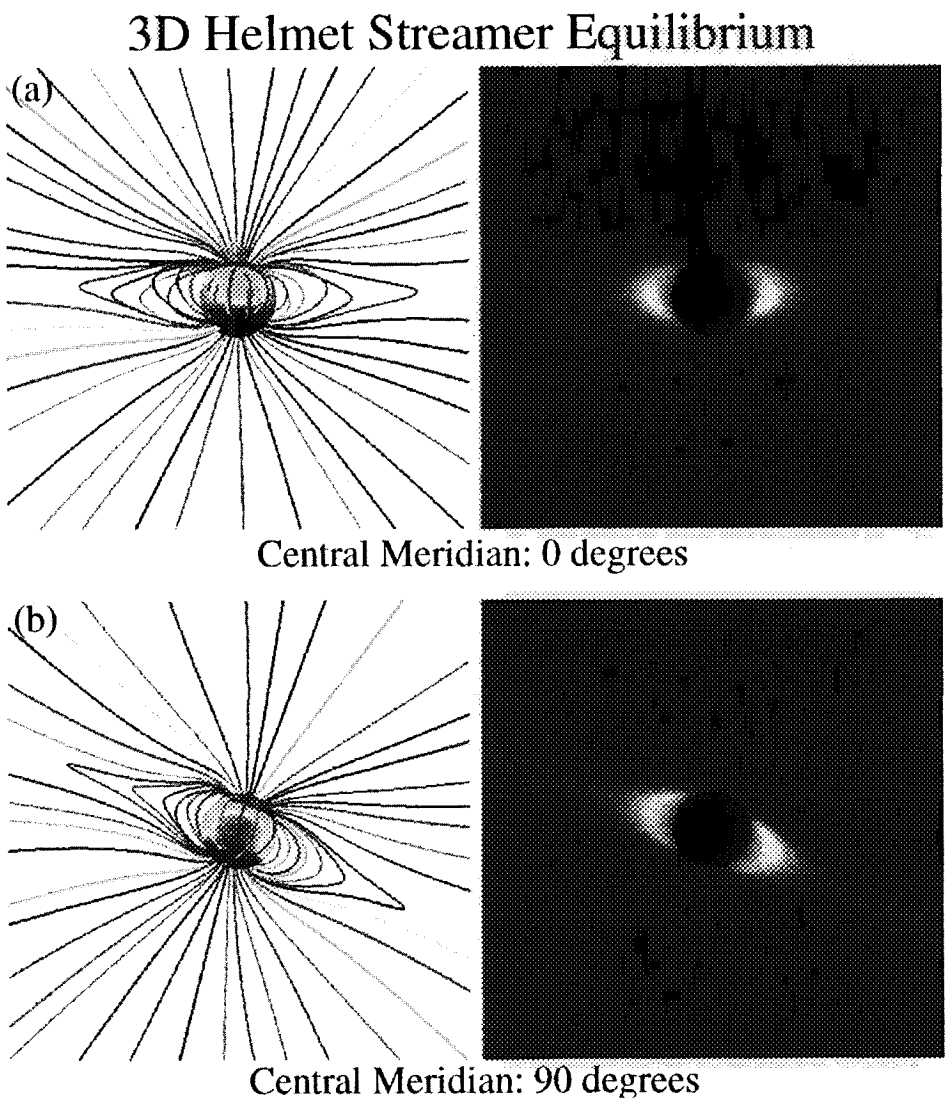

Figure 2. An idealized three-dimensional model of the solar minimum corona. Shown on the left are traces of magnetic field lines; on the right is the corresponding computed plane-of-sky polarization brightness. (a) The view at a central meridian of 0, and (b) the view at a central meridian of 90°. It is apparent that the helmet streamer belt is tilted and warped.

shear is exceeded. With continued differential rotation, the streamer disrupts recurrently [*Linker et al.*, 1994]. A more complete understanding of the role of differential rotation in initiating CMEs requires three-dimensional calculations with more realistic fields, as described below.

5. DISRUPTION OF THREE-DIMENSIONAL CORONAL STREAMERS

The axisymmetric results provide, at best, a qualitative argument that magnetic shear may be a plausible mechanism for the initiation of CMEs. To proceed beyond this qualitative agreement with the properties of CMEs, it will be necessary to compare the details of the eruption with observations (e.g., frequency of eruption, requirements on the photospheric shear profile, the signature of the eruption in coronagraphs, the properties of the plasmoid in interplanetary space). We have already begun this task by studying the propagation of an erupted three-dimensional plasmoid through interplanetary space to 1 A.U. [*Linker and Mikić*, 1997]. Here we present preliminary results on the extension of our studies to the shearing and eruption of three-dimensional helmet streamers.

Our first studies of the evolution and stability of three-dimensional magnetic arcades were made using a zero-beta

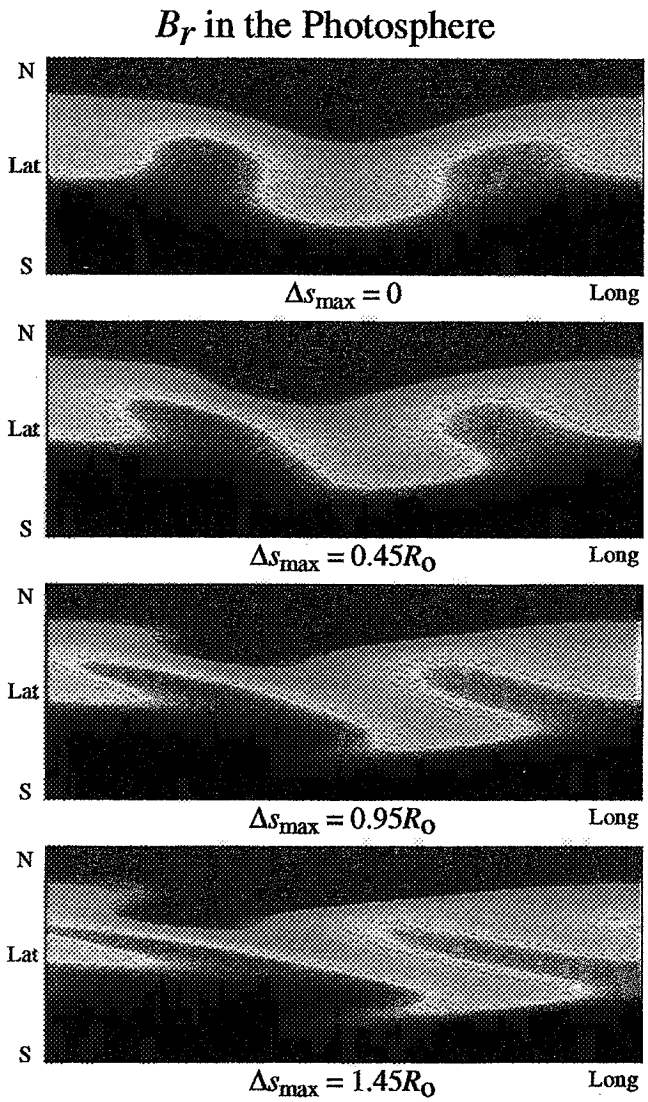

Figure 3. The evolution of the radial component of the magnetic field in the photosphere, B_r, as a function of the maximum footpoint displacement, Δs_{max}. Note that the photospheric flow changes the magnetic flux in the solar surface.

model without the solar wind. The results indicated that arcades erupt beyond a critical shear, as in the axisymmetric case. Here we describe the extension of this model to include the effect of the solar wind. To generate a 3D helmet streamer equilibrium, we first find the potential field in the corona that corresponds to the following radial magnetic field in the photosphere:

$$B_r = B_0(A_0 \cos^3\theta + A_2 \sin^2\theta \cos 2\phi + A_3 \sin^3\theta \sin 3\phi),$$

with $B_0 = 13.3$ Gauss, $A_0 = 1$, $A_2 = 0.1$, and $A_3 = 0.025$, rotated by $-20°$ about the y-axis. Here (r,θ,ϕ) are spherical coordinates: θ is the co-latitude ($\theta = 0$ is the North pole; $\theta = 180°$ is the South pole), and ϕ is the longitude. (The y-axis is the line $\theta = 90°$, $\phi = 90°$.) This is an idealization of the magnetic field at solar minimum, with a warped, asymmetric neutral line and relatively smooth fields, that resembles the large-scale magnetic field for the observational data we have studied, producing a tilted, warped heliospheric current sheet.

The potential field corresponding to this normal field at the photosphere was computed as an initial state, and the resistive MHD equations were integrated to steady state to compute a 3D coronal streamer equilibrium. Figure 2 shows the magnetic field lines in the equilibrium, along with the computed polarization brightness, at two choices of central meridian longitude. It is readily apparent that this is a three-dimensional configuration.

The evolution of this equilibrium was then followed in response to an applied photospheric shear flow. We used an idealized shear profile similar to that used previously for axisymmetric arcades [*Mikić and Linker*, 1994], with $\mathbf{v} = v_\phi(\theta)\hat{\boldsymbol{\phi}}$, and a width $\Delta\theta_m = 30°$. (Note that this profile does not correspond to differential rotation; the evolution of this field for a differential rotation profile is discussed by Linker and Mikić [1997].) In this three-dimensional equilibrium, the normal component of the magnetic field in the photosphere changes as a result of the advection of magnetic flux. Figure 3 shows the evolution of B_r in the photosphere. We parameterize the amount of shear introduced at any particular time in terms of the maximum displacement of a field line footpoint from its initial position, Δs_{max}, as in [*Mikić and Linker*, 1994].

In order to minimize the computational time required to perform this 3D numerical simulation, we used a shear flow velocity that is ~ 10 times larger than flows that are typically observed in the photosphere. The maximum shear flow velocity was 4.8 km/s, compared to typical photospheric flow velocities of 0.5–1 km/s; the photospheric flow velocity associated with solar rotation is 2 km/s. Our previous results [*Mikić and Linker*, 1994] imply that magnetic fields evolve quasi-statically prior to eruption. Our enhanced shear flow velocity is therefore expected to shorten the time required to reach a level of shear that leads to an eruption, and is not expected to affect the nature of the eruption significantly (as long as the shear flow velocity is small compared to the Alfvén speed). It is possible to use a physical value of the shear flow velocity in our simulations (at greater computational expense), and this will be done in future refinements of this calculation.

Figure 4 shows the evolution of selected magnetic field lines as a function of the footpoint displacement. Note that the field lines rise slowly as they become twisted. When the shear reaches a critical value ($\Delta s_{max} \sim 1.6R_0$, where R_0 is the solar radius), the field lines begin to expand outward rapidly. This behavior is qualitatively similar to that observed in the axisymmetric case, although the field

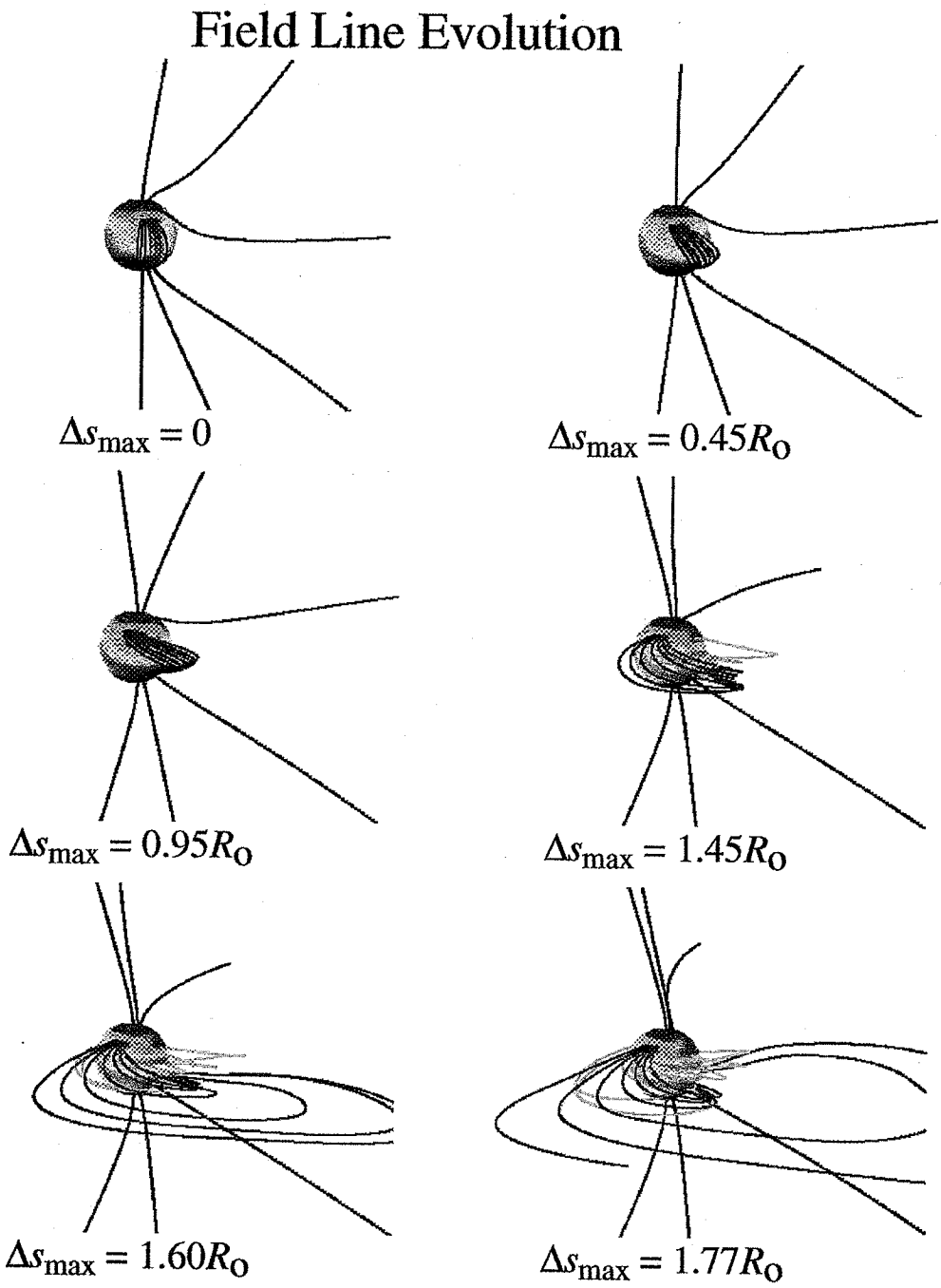

Figure 4. The evolution of selected magnetic field lines in a three-dimensional configuration as a function of the maximum footpoint displacement, Δs_{max}. The field lines initially evolve quasi-statically as they become twisted by the applied photospheric shear flow. However, when the twist approaches $\Delta s_{max} \sim 1.6R_O$, there is a rapid upward motion of the field lines. This eruption is characteristic of a coronal mass ejection.

line geometry is considerably more complicated. The erupting magnetic field lines have a long wavelength structure, indicating that the eruption is global, with a large longitudinal extent. This feature of the eruption agrees with recent LASCO coronagraph images of CMEs, in which CME ejecta appear to leave the East and West solar limbs simultaneously.

The magnetic energy of the configuration decreases following the eruption, as magnetic reconnection takes place. The nature of the reconnection is complicated, and is

not easily diagnosed. (We deduce that reconnection is taking place because the magnetic footpoint connectivity in the photosphere changes rapidly after the eruption.) The magnetic flux that is ejected has been followed as it propagates into interplanetary space in a related simulation [*Linker and Mikić*, 1997].

6. DISCUSSION

We have studied the evolution of 2D and 3D helmet streamer configurations in the presence of photospheric shearing flows. The streamers initially evolve quasi-statically, causing the closed field region to grow in size. When a critical shear is reached, the configurations erupt, sending plasma and magnetic fields into the outer corona. This eruption appears to be an ideal process, related to the tendency of the field to open when the energy of the field approaches the open field energy. Subsequent to this outward eruption of the field lines, reconnection of the magnetic field occurs. The nature of this reconnection process in three dimensions is quite complicated and is presently under investigation.

Our results indicate that magnetic shear may initiate coronal mass ejections. At present, this evidence must be regarded as qualitative, since it is based on the study of idealized magnetic field configurations. In future work it will be necessary to compare the predictions from our theoretical model with available observational data, especially the properties of plasmoids and "flux ropes" observed in the interplanetary medium, to obtain a more quantitative evaluation of the role of magnetic shear in CME initiation.

Acknowledgments. The research described here was supported by NASA, NSF, and AFPL. The computations were performed at the National Energy Research Supercomputer Center and the San Diego Supercomputer Center.

REFERENCES

Aly, J. J., *Ap. J.*, *283*, 349, 1984.
Aly, J. J., *Ap. J.*, *375*, L61, 1991.
Einaudi, G., and G. Van Hoven, *Phys. Fluids*, *24*, 1092, 1981.
Feynman, J., and S. F. Martin, *J. Geophys. Res.*, *100*, 3355, 1995.
Hiei, E., A. J. Hundhausen, and D. G. Sime, *Geophys. Res. Lett.*, *20*, 2785, 1993.
Hudson, H. S., L. W. Acton, D. Alexander, S. L. Freeland, J. R. Lemen, and K. L. Harvey, Yohkoh/SXT Soft X-ray Observations of Sudden Mass Loss from the Solar Corona, in *Solar Wind Eight: Proceedings of the Eight International Solar Wind Conference*, edited by D. Winterhalter, J. T. Gosling, S. R. Habbal, W. S. Kurth, and M. Neugebauer, pp. 88–91, AIP Conf. Proceedings, *382*, AIP Press, Woodbury, N. Y., 1996.
Kopp, R. A., and G. W. Pneuman, *Sol. Phys.*, *50*, 85, 1976.
Leka, K. D., Ph. D. Thesis, University of Hawaii, 1995.
Linker, J. A., and Z. Mikić, *Ap. J.*, *438*, L45, 1995.
Linker, J. A., and Z. Mikić, Extending Coronal Models to Earth Orbit, in *Coronal Mass Ejections: Causes and Consequences* (this volume), 1997.
Linker, J. A., Z. Mikić, and D. D. Schnack, in *Proc. Third SOHO Workshop — Solar Dynamic Phenomena and Solar Wind Consequences*, Estes Park, Colorado, USA (ESA SP-373), 249, 1994.
Linker, J. A., Z. Mikić, and D. D. Schnack, in *Solar Drivers of Interplanetary and Terrestrial Disturbances*, edited by K. S. Balasubramaniam, S. L. Keil, and R. N. Smartt, Astronomical Society of the Pacific, Conference Series, *95*, 208, 1996.
Linker, J. A., G. Van Hoven, and D. D. Schnack, *Geophys. Res. Lett.*, *17*, 2281, 1990.
Lites, B. W., B. C. Low, V. Martínez Pillet, P. Seagraves, A. Skumanich, Z. A. Frank, and R. A. Shine, *Ap. J.*, *446*, 877, 1995.
Mikić, Z., and J. A. Linker, *Ap. J.*, *430*, 898, 1994.
Mikić, Z., and J. A. Linker, The Large-Scale Structure of the Solar Corona and Inner Heliosphere, in *Solar Wind Eight: Proceedings of the Eight International Solar Wind Conference*, edited by D. Winterhalter, J. T. Gosling, S. R. Habbal, W. S. Kurth, and M. Neugebauer, pp. 104–107, AIP Conf. Proceedings, *382*, AIP Press, Woodbury, N. Y., 1996.
Mikić, Z., J. A. Linker, and D. D. Schnack, in *Solar Drivers of Interplanetary and Terrestrial Disturbances*, edited by K. S. Balasubramaniam, S. L. Keil, and R. N. Smartt, Astronomical Society of the Pacific, Conference Series, *95*, 108, 1996.
Mikić, Z., and A. N. McClymont, in *Solar Active Region Evolution: Comparing Models with Observations*, edited by K. S. Balasubramaniam and G. W. Simon, Astronomical Society of the Pacific, Conference Series, *68*, 225, 1994.
Parker, E. N., *Interplanetary Dynamical Processes*, Wiley-Interscience, New York, 1963.
Parker, E. N., *Ap. J.*, *174*, 499, 1972.
Parker, E. N., *Cosmical Magnetic Fields*, 841 pp., Clarendon, Oxford, 1979.
Pneuman, G. W., and R. A. Kopp, *Sol. Phys.*, *18*, 258, 1971.
Priest, E. R., in *Solar Flare Magnetohydrodynamics*, edited by E. R. Priest, Gordon and Breach, London, 1981.
Priest, E. R., *Solar Magnetohydrodynamics*, 469 pp., Reidel, Dordrecht, 1982.
Raadu, M. A., *Sol. Phys.*, *22*, 425, 1972.
Roumeliotis, G., P. A. Sturrock, and S. K. Antiochos, *Ap. J.*, *432*, 847, 1994.
Snodgrass, H. B., *Ap. J.*, *270*, 288, 1983.
Steinolfson, R. S., S. T. Suess, and S. T. Wu, *Ap. J.*, *255*, 730, 1982.
Sturrock, P.A., *Ap. J.*, *380*, 655, 1991.
Tsuneta, S., *Ap. J.*, *464*, 1055, 1996.
Vainshtein, S. I., and E. N. Parker, *Ap. J.*, *304*, 821, 1986.
Wang, A. H., S. T. Wu, S. T. Suess, and G. Poletto, *Sol. Phys.*, *147*, 55, 1993.

Zoran Mikić and Jon A. Linker, Science Applications International Corporation, 10260 Campus Point Drive, San Diego, CA 92121

Extending Coronal Models to Earth Orbit

Jon A. Linker and Zoran Mikić

Science Applications International Corporation, San Diego, California

Solar wind conditions at Earth play a primary role in the initiation of geomagnetic activity. The forecasting of solar wind conditions at Earth based on remote observations of the Sun is thus a key element of space weather prediction. We describe how observations of the photospheric magnetic field can be incorporated into three-dimensional MHD computations of the solar corona and inner heliosphere. We show that the resulting solutions compare favorably with observations and that this same capability can be used to model the initiation of coronal mass ejections and their propagation out into the heliosphere. These encouraging results suggest that an operational computational solar wind model can eventually be developed, suitable for forecasting solar wind properties at Earth.

1. INTRODUCTION

Coronal mass ejections (CMEs) are exceedingly complex phenomena. From their initiation on the Sun to their propagation through the heliosphere, CMEs span a large range of both distance and physical parameter space. Understanding how CMEs, typically observed as loop-like structures in white-light coronagraphs [e.g., *Hundhausen*, 1993], are initiated and how they ultimately manifest themselves in interplanetary space is a fundamental challenge for solar and heliospheric science. Apart from the intellectual attraction of such a challenge, solution of this problem has significant practical applications. It is well known that solar wind conditions upstream of the Earth's magnetosphere play an important role in geomagnetic activity, and that CMEs in particular are associated with the largest geomagnetic storms [*Gosling*, 1993]. Geomagnetic storms can cause disruption of satellite operations, communications, navigation, and electric power distribution grids, and create a hazardous environment for astronauts engaged in extra-vehicular activities. The prediction of such "space weather" phenomena has thus become recognized as an important problem for the space science community, as evidenced by the National Space Weather Program Strategic Plan [*Wright et al.*, 1995].

Remote observations of the magnetic and plasma environment of the Sun have been made routinely for some time. With the SOHO spacecraft now operational, the amount and quality of such measurements, including the detection of CMEs, has greatly increased. In the context of space-weather forecasting, using remote solar observations to accurately predict the characteristics of the solar wind at Earth orbit, especially the arrival time and properties of CMEs, is one of the primary services to be provided by solar and heliospheric science.

To predict effects at Earth from events occurring on the Sun, solar observations must be incorporated into a physical model. The magnetohydrodynamic (MHD) fluid description is an appropriate starting point for modeling the solar wind. Even with multi-fluid and kinetic effects neglected, consideration of the important physical processes in multi-dimensional geometry renders the MHD equations intractable to an analytic approach, and a computational solar wind model is necessary if we are to forecast solar wind conditions at Earth orbit. This is not surprising, as computational models of the atmosphere have long played an important

Coronal Mass Ejections
Geophysical Monograph 99

role in terrestrial weather prediction [*Houghton*, 1977]. Our computational solar wind model must fulfill two requirements: (1) computation of the "background" solar corona and solar wind, and (2) calculation of the initiation and propagation of CMEs. Requirement (1) arises because the geoeffectiveness of CMEs is related to the structure of the interplanetary magnetic field (IMF) [*Gosling et al.*, 1990]; [*Crooker et al.*, 1992]. Also, apart from the effect of CMEs, the background solar wind plays an important role in geomagnetic activity. It has long been known that 27 day recurrences in geomagnetic activity are directly linked to the solar rotation period [e.g., *Maunder*, 1905]. Fast streams in the solar wind, which originate in coronal holes [e.g., *Altschuler et al.*, 1972], are generally believed to be the cause of recurrent geomagnetic storms [*Hundhausen*, 1979; *Zirin*, 1988; *Foukal*, 1990]. Recently the role of the streamer belt and corotating interaction regions in producing recurrent geomagnetic activity has also been recognized [*Crooker and Cliver*, 1994].

At the outset, we must recognize the formidable nature of the goal we have described and how distant we are from achieving it. While many obstacles contribute to the difficulty of solar wind forecasting, perhaps the most obvious problem is our lack of understanding of how CMEs are initiated. Nevertheless, to make progress on this task, we must outline a strategy for model development. With this purpose in mind, we demonstrate in this paper how MHD models of the solar wind can supply the two key requirements for solar wind forecasting. Section 2 briefly discusses the methodology of our computations. In section 3 we describe realistic computations of the solar corona, and we show that our results compare favorably with coronal and heliospheric observations. In sections 4 and 5 we demonstrate a model computation of the solar corona and inner heliosphere at solar minimum, and we show how one candidate process for CME initiation (shearing of the magnetic footpoints by differential rotation) can be modeled and the heliospheric effects of the resulting disturbance studied. Section 6 summarizes our present capabilities and indicates future directions.

2. METHODOLOGY

To compute MHD solutions for the large-scale corona, we solve the following form of the equations in spherical coordinates:

$$\nabla \times \mathbf{B} = \frac{4\pi}{c}\mathbf{J} \tag{1}$$

$$\frac{1}{c}\frac{\partial \mathbf{B}}{\partial t} = -\nabla \times \mathbf{E} \tag{2}$$

$$\mathbf{E} + \frac{\mathbf{v} \times \mathbf{B}}{c} = \eta \mathbf{J} \tag{3}$$

$$\frac{\partial \rho}{\partial t} + \nabla \cdot (\rho \mathbf{v}) = 0 \tag{4}$$

$$\rho\left(\frac{\partial \mathbf{v}}{\partial t} + \mathbf{v} \cdot \nabla \mathbf{v}\right) = \frac{1}{c}\mathbf{J} \times \mathbf{B} - \nabla p - \nabla p_w + \rho \mathbf{g} + \nabla \cdot (\nu \rho \nabla \mathbf{v}) \tag{5}$$

$$\frac{\partial p}{\partial t} + \nabla \cdot (p\mathbf{v}) = (\gamma - 1)(-p \nabla \cdot \mathbf{v} + S) \tag{6}$$

where $\mathbf{B}$ is the magnetic field intensity, $\mathbf{J}$ is the electric current density, $\mathbf{E}$ is the electric field, $\mathbf{v}$, ρ, and p are the plasma velocity, mass density, and pressure. The gravitational acceleration is $\mathbf{g}$, γ is the ratio of specific heats, η is the resistivity, ν is the viscosity, S represents energy source terms, and the wave pressure p_w represents the acceleration due to Alfvén waves [*Jacques*, 1977; *Holweg*, 1978].

The term S in equation (6) includes the effects of coronal heating, thermal conduction parallel to $\mathbf{B}$, radiative losses, and Alfvén wave dissipation (viscous and resistive dissipation can also be included). A simplified model of the corona, known as the "polytropic model", is obtained when an adiabatic energy equation with a reduced γ is used [*Parker*, 1963]. This is a crude way of modeling the complicated thermodynamics in the corona with a simple energy equation. This choice results by setting $S = 0$ in Eq. (6) and $p_w = 0$ in Eq. (5). With this model, values of γ close to 1 ($\gamma = 1.05$ for the results shown in this paper) are necessary to produce density and temperature profiles that are similar to coronal observations; this indicates that the terms included in S are in fact important for describing the energy balance of the corona. In this paper we describe computations using the polytropic model. Computations using the full equations (1–6) have been performed [*Mikić et al.*, 1996ab] and will be described in a future paper.

Mikić and Linker [1994] describe the method used to solve equations (1–6). To compute coronal and heliospheric solutions, the equations must be supplemented with appropriate boundary and initial conditions. In spherical geometry, two boundaries appear in the simulation: the physical inner radial boundary at r = R_s (the solar radius) and an artificial outer radial boundary at r = R_1, which we typically place in the range 20–215 R_s.

Specification of the appropriate boundary conditions is facilitated by examining the characteristic form of equations (1-6) [*Courant and Friedrichs*, 1948]. (See *Hu and Wu*, [1984] for an example using the MHD equations.) Characteristics traveling into the domain require that physical information be provided. At the inner boundary, four characteristics point into the domain, and require that four quantities be specified. We specify the distributions of ρ and p at r = R_s. When no surface motions are included in the calculation, we also specify that E_θ and $E_\phi = 0$ at r = R_s; this condition fixes the radial magnetic field at the inner boundary (B_{r0}) at its initial value and is equivalent to setting $\mathbf{v}_\perp$ (velocity perpendicular to $\mathbf{B}$) = 0 there. When surface motions such as the solar rotation are included, E_θ and E_ϕ are specified to be consistent with this motion (from equation 3); note that in this case the distribution of B_{r0} can be modified by the surface motions. The outer boundary is typically placed well beyond the critical points, so all characteristics are outgoing and no physical boundary conditions are required. To advance the solution at the outer boundary, we use the characteristic equations to compute $\mathbf{v}$. The plasma β ($= 8\pi p/B^2$, the ratio of plasma pressure to magnetic pressure) is typically 1 or greater at the outer boundary, and we find that characteristics based on the gas equations are sufficient. The staggering of the mesh then allows all other quantities to be computed in the same manner as the interior points [*Mikić and Linker*, 1994]. Characteristic equations are also used to compute $\mathbf{v}_\parallel$ (velocity parallel to $\mathbf{B}$) at the lower boundary.

For the initial condition, a potential magnetic field consistent with the specified distribution of B_r at the lower boundary, and a wind solution [*Parker*, 1963] consistent with the specified ρ and p are used. Equations (1-6) are then integrated forward in time until a steady state is reached. The computations are performed on a mesh that is nonuniform in the r and θ directions: $\Delta r \approx .01$ R_s near the inner boundary and $\Delta r \approx 10$ R_s at r = 215 R_s; $\Delta\theta$ varied between .03 and .06 radians. The longitudinal (ϕ) coordinate is treated using a pseudospectral method (this requires a uniform distribution of points in ϕ). Our higher resolution cases used 101 × 101 × 64 (r,θ,ϕ) points; cases extending out to approximately 1 A.U. (1 astronomical unit = 1.49 × 10^6 km = 214 solar radii) used 111 × 51 × 32 points.

Previous coronal and solar wind solutions of (1-6) have typically been performed with idealized magnetic fields [*Endler*, 1971; *Pneuman and Kopp*, 1971; *Steinolfson et al.*, 1982; *Washimi et al.*, 1987; *Linker et al.*, 1990; *Wang et al.*, 1993; *Linker and Mikić*, 1995], or with an inner boundary beyond the critical points [*Smith and Dryer* 1990; *Detman et al.*, 1991; *Pizzo*, 1991; *Odstrcil*, 1994]. To perform a realistic 3-D MHD computation of the corona that can be compared with specific observations, it is necessary to incorporate solar observations into the boundary conditions [*Usmanov*, 1993; *Mikić and Linker*, 1996; *Linker et al.*, 1996]. One of the most readily available observational data sets is the magnetic field at the photosphere. This is also the most important observation to address for coronal and heliospheric modeling. We have used Wilcox Solar Observatory synoptic maps (collected during a solar rotation by daily measurements of the line-of-sight magnetic field at central meridian) to specify the radial magnetic field at the photosphere (in the manner described by *Wang and Sheeley* [1992]).

3. COMPARISONS WITH CORONAL AND HELIOSPHERIC DATA

Solutions obtained in the manner described in section 2 can in principle provide a 3D description of the corona and inner heliosphere, including the detailed distribution of magnetic fields, currents, plasma density, and temperature. However, the validity of this approach can only be verified through comparison with observations. As a test of our coronal modeling capability, we used our computations to predict the large-scale structure of the solar corona during the October 24, 1995 eclipse (occurring during Carrington rotation (CR) 1901), visible in a number of locations in the eastern hemisphere. We carried out a simulation using photospheric magnetic field data from the previous rotation (CR1900; September 2 – September 29, 1995) on October 5, 1995, and put the results on the World Wide Web (more detailed comparisons and new results can be viewed at http://iris023.saic.com:8000/corona/modeling.html). We also presented the results at the Sacramento Peak workshop on October 18, 1995 [*Linker et al.*, 1996]. Figure 1 (leftmost frame) shows the magnetic field lines from our calculation. The view angle corresponds to the approximate time of the eclipse. The solution shows the formation of helmet streamers; these are regions with closed magnetic fields that trap coronal plasma flowing out of the Sun. Along open magnetic field lines, the solar wind streams freely, reaching supersonic speeds.

To directly compare our results with observations, we develop images of the polarization brightness (pB; pro-

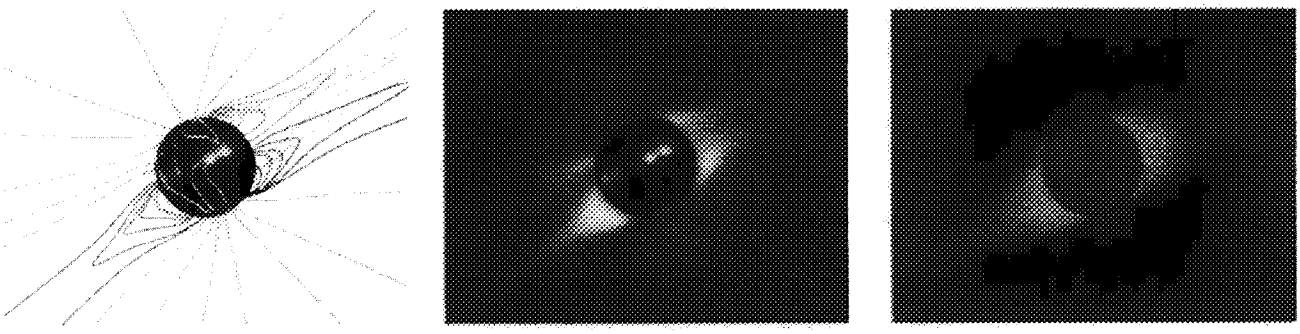

Figure 1. A prediction of the structure of the solar corona during the October 24, 1995 solar eclipse. The MHD simulation was carried out on October 5, 1995, using Wilcox synoptic magnetic data for the previous rotation. From left to right, the frames show: Field lines, polarization brightness computed from the simulation, and an eclipse photograph taken by F. Diego (UCL) in white light with F=910 mm and a two-second exposure time.

portional to the line-of-sight integral of the product of the electron density and a scattering function that varies along the line of sight). This quantity is frequently observed with coronagraphs. Using the plasma density from our coronal model, we can compute pB to simulate an eclipse or coronagraph image and compare it with the actual data. Radially graded filters are applied to eclipse images to compensate for the rapid fall-off of coronal density with radial distance; we detrend our computed pB in a similar manner. The polarization brightness of the corona predicted by our simulation, as it would be seen on October 24, 1995, at 05:00UT is shown in Figure 1 (middle frame), along with an image of the eclipse taken by F. Diego of University College, London (rightmost frame). The helmet streamers and open field regions predicted by the computation agree reasonably well with the eclipse observations. We have performed a similar comparison for the November 3, 1994 eclipse and CR1888 [*Mikić and Linker*, 1996; *Linker et al.*, 1996]. These computations support the long-held belief that the magnetic field distribution on the Sun controls the position and shape of the streamer belt.

We have also compared the results of our calculations with interplanetary observations. As a first test, we computed an MHD model of the solar corona for CR1869 (May–June 1993). This rotation was of particular interest for Ulysses observations, as the Ulysses spacecraft ceased to observe sector-boundary crossings during that time period [*Smith et al.*, 1993]. Figure 2 shows a comparison of the heliospheric current sheet (HCS) predicted by our MHD computation with that of the source-surface model [e.g., *Schatten et al.*, 1969; *Altschuler and Newkirk*, 1969; *Hoeksema*, 1991; *Wang and Sheeley* 1988, 1992], a frequently used tool for approximating heliospheric structure. Ulysses' latitude position for this time period (near 30° S latitude) is also shown. The source-surface model predicts crossings for this time period, whereas the MHD simulation correctly predicts no HCS crossings.

During February–April of 1995 (before and after the spacecraft approached perihelion), the Ulysses spacecraft sampled a wide range of heliographic latitude in a short period of time. Figure 3 shows the HCS predicted by our MHD computation for CR1892, the start of this fast latitude scan. Also shown is the Ulysses trajectory projected in solar latitude and Carrington longitude (back at the Sun) and published Ulysses HCS crossings indicated by crosses [*Smith et al.*, 1995]. The different line styles on the trajectory plots indicate the Carrington rotation at that time. During CR1892 (the time period for which the calculation is most valid), the two Ulysses crossings occur almost exactly where predicted by the MHD computation. Later in time (CR1893 and CR1894), the overall shape of the MHD HCS agrees well with Smith et al.'s empirically derived HCS, but the Ulysses crossings occur above the MHD HCS. The reason for this can be seen in Figure 4, which shows the predicted source-surface model for the 3 rotations. The source-surface model suggests that the solar magnetic field is changing during this time period, as evidenced by the changing HCS. Therefore, MHD computations of CR1893 and CR1894 are required for a complete comparison; this work is presently underway.

While the favorable comparisons between our computational results and coronal and heliospheric observations are encouraging, it should be noted that there

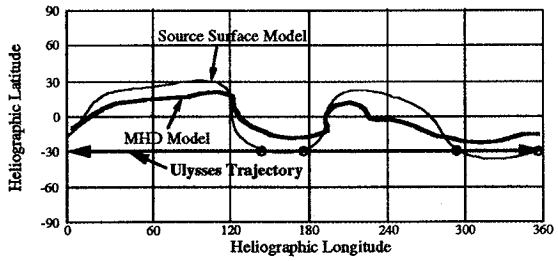

Figure 2. A comparison of the heliospheric current sheet predicted by the source-surface model and an MHD calculation for Carrington rotation (CR) 1869 (May10–June 6, 1993). The Ulysses spacecraft, which did not observe current sheet crossings during this rotation, was situated at 30° latitude. The circles indicate the crossings predicted by the source-surface model.

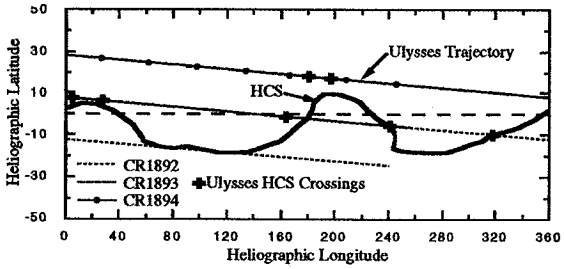

Figure 3. The heliospheric current sheet (HCS) predicted by the MHD model for CR1892, with the Ulysses trajectory for the fast-latitude scan superimposed. HCS crossings identified by *Smith et al.* [1995] are indicated by black crosses. The times of the different rotations (CR1892, CR1893, and CR1894) are coded by line style on the trajectory plot.

are also some differences between our simulations and observations. Fine-scale details of the corona do not appear in our computations. Higher resolution magnetograms (such as those from the National Solar Observatory at Kitt Peak or the SOI/MDI instrument aboard SOHO), coupled with higher resolution computations, may help to capture some of these fine-scale features. Streamers in eclipse images typically show a stronger nonradial tendency than in our the computations. This may be related to the poor estimation of polar fields in the Wilcox data, due to projection effects, and may also be improved by better magnetograms. Most important, our computations (using a polytropic model) fail to reproduce the fast (800km/s) solar wind observed by Ulysses at high latitude. Improvement of this aspect of the calculation requires consideration of the momentum and energy source terms discussed in section 2. Our preliminary 1D and 2D calculations including these terms

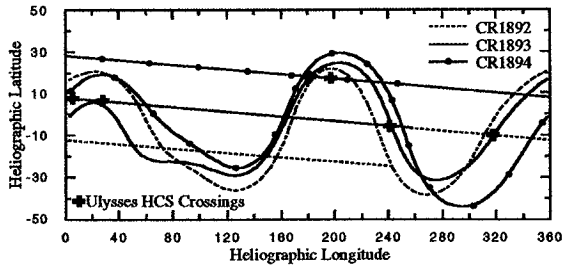

Figure 4. Variation of the heliospheric current sheet predicted by the source-surface model for the rotations occuring during the fast-latitude scan. The extent of the HCS varies during this time period.

show promising results [*Mikić et al.*, 1996ab], and further investigation of these solutions is ongoing.

4. A MODEL OF THE CORONA AND INNER HELIOSPHERE AT SOLAR MINIMUM

To demonstrate how CMEs may be initiated in the corona and propagate out into the heliosphere, we developed a model configuration of the solar corona (and its extension to 1 A.U.) at solar minimum. Guided by our experience with the Wilcox photospheric magnetic field data and our comparisons with eclipse images, we specified an initial magnetic flux distribution of the form:

$$B_r = A_0\cos^3\theta + A_1\sin^2\theta\cos2\phi + A_2\sin^3\theta\sin3\phi \quad (7)$$

with A_0 = 13.3 G (Gauss), A_1 = 1.3 G, A_2 = 0.33 G, and the distribution rotated by -20° around the y axis. We then computed an equilibrium configuration by integrating the MHD equations to steady state, as described in section 2, with the additional constraint that the Sun's rigid rotation rate was imposed (corresponding to a sidereal period of 26 days). The resulting configuration is shown in Figure 5. The magnetic field lines and polarization brightness near the Sun (Fig. 5a and 5b) show a configuration similar to that often seen at solar minimum. As we move farther from the Sun, the magnetic field lines show the expected spiral behavior (Figure 5d shows the field lines out to 1 A.U.). With this configuration, we can investigate how different processes can affect coronal evolution, how CMEs might be initiated, and the heliospheric consequences of these events.

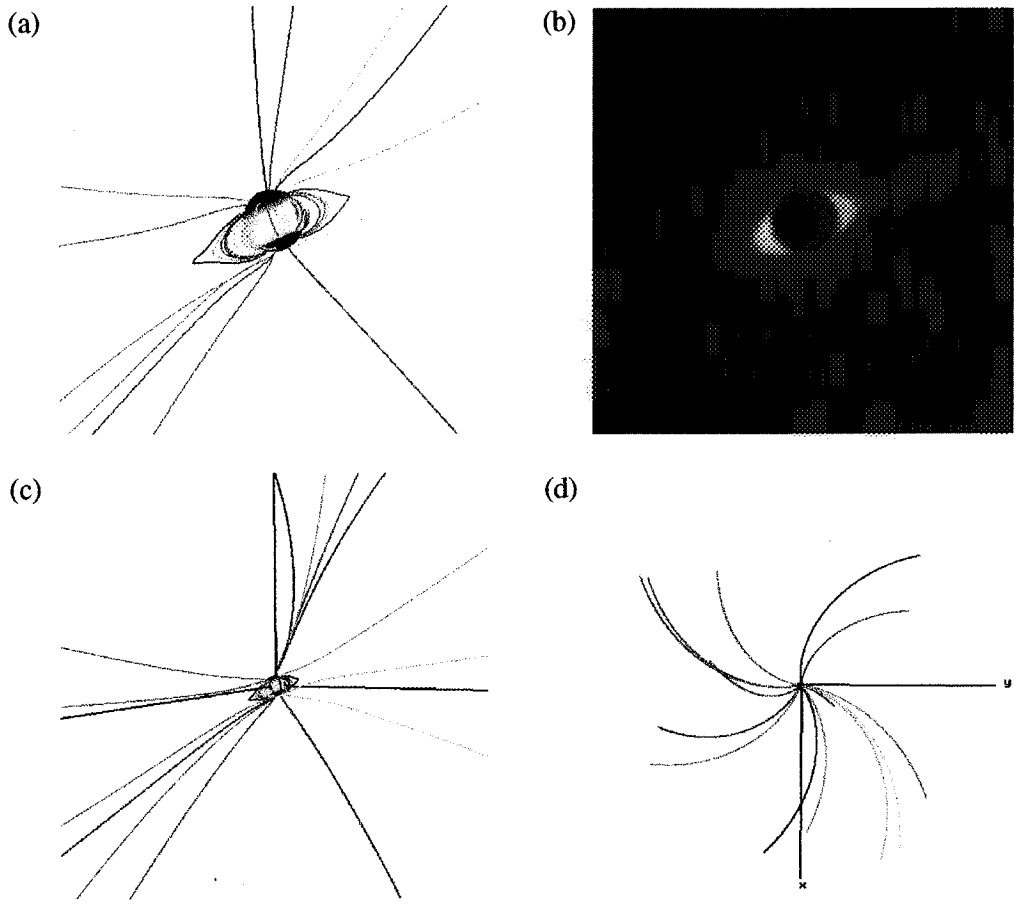

Figure 5. An MHD simulation of the solar corona and inner heliosphere for a solar-minimum type configuration. The computation is performed in the inertial frame, so the magnetic flux distribution on the Sun rotates rigidly. (a) Field lines viewed close to the Sun, showing a helmet streamer configuration. (b) polarization brightness from the same view as (a). (c) Field lines from the same view angle as (a) and (b), but farther from the Sun. (d) Field lines from 1 A.U. above the Sun's North pole. The spiral structure is apparent. Field lines that appear "shorter" actually are receding from or approaching the viewpoint.

5. MODELING CME INITIATION AND PROPAGATION

While the exact cause of CMEs is unknown, it is generally agreed that the amount of energy in the coronal magnetic field (above the energy of the corresponding potential field) is an important factor in determining if and when the coronal magnetic field erupts. Unfortunately, line-of-sight magnetograms do not contain information about the amount of parallel current that is flowing in the coronal magnetic field, so we do not know the magnetic energy state of the corona from these measurements. As is well known from studies of active regions, a vector magnetogram is required to uniquely specify the field. Full-disk vector magnetograms, if available with sufficient accuracy, could allow us to compute coronal configurations that match the measured twist (or shear) in the photospheric magnetic field and determine the magnetic energy state of the corona. Lacking this information, the coronal equilibria we compute (such as those shown in Figure 1 and 5) correspond to helmet streamers with a minimum amount of twist in the magnetic field and probably have an unrealistically low magnetic energy.

One process that might initiate CMEs is shearing of the magnetic field footpoints by photospheric motions [*Mikić and Linker*, 1994; *Linker et al.*, 1994; *Romeliotis*, 1994; *Linker and Mikić*, 1995]. *Mikić and Linker* [this volume] describe how an idealized photospheric shear profile causes the coronal configuration of Figure

5 to evolve, resulting in eruption of a portion of the closed field lines. Because the calculation is starting with a magnetic field that is in a much lower energy state than the actual corona, an artificially long shearing time is necessary to initially energize the field. As we have shown previously [*Linker et al.* 1994; *Linker and Mikić*, 1995], after a sheared helmet streamer erupts, re-formation of the helmet streamer by magnetic reconnection releases only a portion of the available magnetic energy and does not return the configuration to the pre-sheared state. Subsequent eruptions thus require less shear.

Here we discuss a computation where a differential rotation profile, rather than the idealized shear profile described by *Mikić and Linker* [this volume], was introduced. To accomplish the initial energization of the field more rapidly (and reduce computing time), the rotation rate of the Sun was increased by a factor of 10 when we introduced differential rotation. The resulting disruption of the helmet streamer configuration was similar to that described by *Mikić and Linker* [this volume]. The introduction of shear initially causes the magnetic field to expand slowly. When a critical shear is reached, the magnetic field erupts rapidly outward, followed by reconnection of magnetic field lines. In this respect our 3D results are similar to previous 2D results [*Linker et al.*, 1994; *Linker and Mikić*, 1995], but the evolution of the magnetic field in 3D, particularly the magnetic reconnection, is more complicated. As an example of how we can investigate the heliospheric consequences of such eruptions, Figure 6 shows the magnetic field line evolution out to 0.5 A.U. (a portion of the total simulation domain). The black field lines extend out to 1 A.U. in the equilibrium shown in Figure 5; note that the artificially increased rotation rate of the Sun increases the spiral angle for these field lines. A magnetic eruption at t = 44 hours results in a portion of the helmet streamer of Figure 5 expanding rapidly outward into the heliosphere (the gray field lines). A subsequent eruption beginning at t = 76 hours results in more magnetic flux being carried out into the heliosphere.

In the simpler geometry of the previously mentioned 2D studies, a completely detached plasmoid (a torus surrounding the Sun) propagated outward. In the more complicated 3D case shown here, no magnetic field lines that are completely detached from the Sun are apparent, but their presence has not yet been ruled out. These calculations represent our first efforts to investigate coronal mass ejections in three dimensions and should only be regarded as a first step. We plan in further studies to examine the details of the magnetic topology both in the corona and far from the Sun, as well as studying other possible initiation mechanisms.

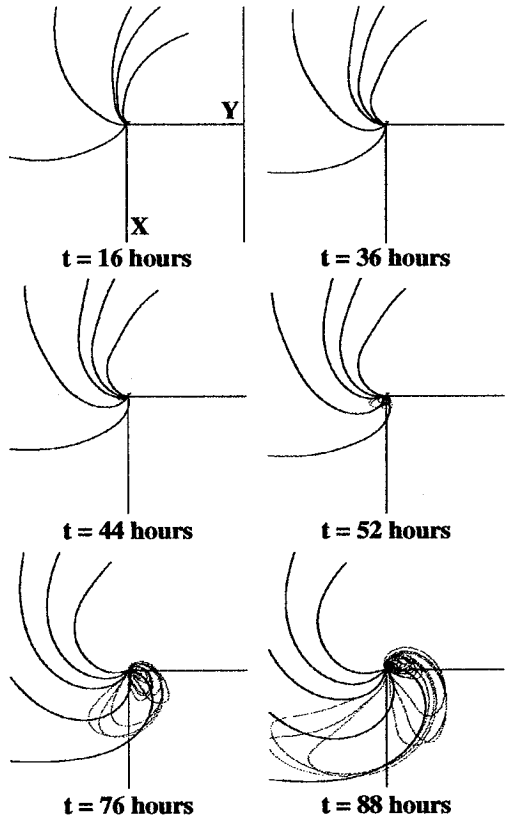

Figure 6. Evolution of magnetic field lines viewed from above the Sun's north pole at 0.5 A.U., after the solar-minimum configuration of Figure 5 is subjected to an enhanced differential rotation profile. Black field lines were open in the initial configuration; gray field lines were initially part of the closed-field helmet streamers. Magnetic eruptions at 44 hours and again at 76 hours cause magnetic flux that previously closed near the Sun to be carried out into the heliosphere.

6. SUMMARY

An important element of predicting geomagnetic activity is forecasting solar wind conditions at Earth orbit. Essential to this effort is a computational model of the solar wind capable of describing (1) the structure of the solar corona and inner heliosphere, and (2) the initiation and propagation of coronal mass ejections.

We have described an MHD model that can in principle provide these capabilities. The favorable comparisons of our model with coronal and heliospheric data indicate that the first of these goals is the most feasible, although a more sophisticated treatment of energy transport in the solar wind is necessary to accurately compute solar wind velocities. The second goal is the more difficult task, since our present understanding of CMEs and their initiation is limited. Simulations like those we have described are an attempt to understand the basic phenomena of CMEs. With the SOHO mission now operational and with continued Yohkoh and ground-based observations, the next few years should see a rapid growth in our knowledge of CMEs. The confluence of improved observations and more sophisticated theory and modeling may lead to an improved understanding of CMEs and, eventually, to the capability to forecast CME effects at the Earth.

Acknowledgments. We would like to thank the Wilcox Solar observatory for the use of their synoptic charts, and Serge Koutchmy for providing us with the October 24, 1995 eclipse photograph shown in Figure 1. We also thank Daniel Winterhalter of JPL for providing us with the Ulysses trajectory. This research was supported by NASA, NSF, and AFPL; computations were performed at the San Diego Supercomputer Center and at the National Energy Research Supercomputer Center.

REFERENCES

Altschuler, M. D., D. E. Trotter and F. Q. Orral, *Sol. Phys.*, *26*, 354, 1972.

Altschuler, M. D., and G. Newkirk, *Sol. Phys.*, *9*, 131, 1969.

Courant, R., and K. O. Friedrichs, *Supersonic Flow and Shock Waves*, Interscience Publishers, New York, 1948.

Crooker, N. U., E. W. Cliver and B. T. Tsurutani, *Geophys. Res. Lett.*, *19*, 429, 1992.

Crooker, N. U. and E. W. Cliver, *J. Geophys. Res.*, *99*, 23383, 1994.

Detman, T. R., M. Dryer, T. Yeh, S. M. Han, S. T. Wu and D. J. McComas,*J. Geophys. Res.*, *96*, 9531, 1991.

Endler, F., *Interaction between the Solar Wind and Coronal Magnetic Fields*, Ph.D. Thesis,Gottingen Univ.,1971.

Foukal, P., *Solar Astrophysics*, Wiley-Interscience, New York, 1990.

Gosling, J. T., S. J. Bame, D. J. McComas and J. L. Philips, *Geophys. Res. Lett.*, *17*, 901, 1990.

Gosling, J. T., *J. Geophys. Res.*, *98*, 18937, 1993.

Hoeksema, J. T., Tech. Rep. CSSA-ASTRO-91-01, Center for Space Science and Astronomy, Stanford University, California, 1991.

Holweg, J. V., *Rev. Geophys. Space Phys.*, *16*, 689, 1978.

Houghton, J. T., *The Physics of Atmospheres*, Cambridge University Press, Cambridge, 1977.

Hu, Y. Q. and S. T. Wu, *J. Comp. Phys.*, *55*, 33, 1984.

Hundhausen, A. J., *Rev. Geophys.*, *17*, 2034, 1979.

Hundhausen, A. J., *J. Geophys. Res.*, *98*, 13177, 1993.

Jacques, S. A., *Astrophys. J.*, *215*, 942, 1977.

Linker, J. A., G. Van Hoven and D. D. Schnack, *Geophys. Res. Lett.*, *17*, 2281, 1990.

Linker, J. A. and Z. Mikić, *Astrophys. J.*, *438*, L-45, 1995.

Linker, J. A., Z. Mikić and D. D. Schnack, in *Solar Drivers of Interplanetary and Terrestrial Disturbances*, (K. S. Balasubramaniam, S. L. Keil, and R. N. Smartt, eds.), Astron. Soc. Pac. Conf., *95*, 208, 1996.

Linker, J. A., Z. Mikić and D. D. Schnack, in *Solar Dynamic Phenomena and Solar Wind Consequences*, Proc. Third SOHO Workshop, Estes Park, Colorado, (ESA SP-373), 249, 1994.

Maunder, E. W., *Mon. Not. R. Astron. Soc.*, *65*, 2, 1905.

Mikić, Z. and J. A. Linker, *Astrophys. J.*, *430*, 898, 1994.

Mikić, Z., and J. A. Linker, *Solar Wind 8*, AIP Conf. Proceedings 382, 104, 1996.

Mikić, Z., and J. A. Linker, this volume.

Mikić, Z., J. A. Linker and J. A. Colborn, *EOS Trans. AGU* (abstract), *77*, 1996a.

Mikić, Z., J. A. Linker and J. A. Colborn, AAS/SPD Meeting (abstract), Madison, Wisconsin, 1996b.

Odstrcil, D., *J. Geophys. Res.*, *99*, 17653, 1994.

Parker, E. N., *Interplanetary Dynamical Processes*, Interscience Publishers, New York, 1963.

Pizzo, V., *J. Geophys. Res.*,*96*, 5405, 1991.

Pneuman, G. W. and R. A. Kopp, *Solar Phys.*, *18*, 258, 1971.

Roumeliotis, G., P. A. Sturrock, and S. K. Antiochos, *Astrophys. J.*, *432*, 847,1994.

Schatten, K. H., J. M. Wilcox and N. Ness, *Solar Phys.*, *6*, 442, 1969.

Smith, Z., and M. Dryer, *Solar Phys.*, *129*, 1990.

Smith, E. J., M. Neugebauer, A. Balogh, S. J. Bame, G. Erdos, R. J. Forsyth, B. E. Goldstein, J. L.Phillips and B. Tsurutani, *Geophys. Res. Lett.*, *20*, 2327, 1993.

Smith, E. J., A. Balogh, M. E. Burton, G. Erdos and R. J. Forsyth, *Geophys. Res. Lett.*, *22*, 3325, 1995.

Steinolfson, R. S., S. T. Suess and S. T. Wu, *Astrophys. J.*, *255*, 730, 1982.

Usmanov, A. V., *Solar Phys.*, *146*, 207, 1993.

Wang, A. H., S. T. Wu, S. T. Suess and G. Poletto, *Sol. Phys.*, *147*, 55, 1993.

Wang, Y. M. and N. R. Sheeley, *J. Geophys. Res.*, *93*, 11, 227, 1988.

Wang, Y. M. and N. R. Sheeley, Jr., *Astrophys. J.*, *392*, 310, 1992.

Washimi, H., Y. Yoshino and T. Ogino, *Geophys. Res. Lett.*, *14*, 487, 1987.

Wright, J. M., Jr., et al., *National Space Weather Progrom Strategic Plan*, FCM-P30-1995, 1995.

Zirin, H., *Astrophysics of the Sun*, Cambridge University Press, New York, 1988.

Jon A. Linker and Zoran Mikić, Science Applications International Corporation, San Diego, CA 92121.

REPORT DOCUMENTATION PAGE

Form Approved
OMB No. 0704-0188

1. AGENCY USE ONLY *(Leave blank)*	2. REPORT DATE	3. REPORT TYPE AND DATES COVERED
	June 19, 1998	Interim for 07/26/96 - 07/15/97

4. TITLE AND SUBTITLE
The Structure and Dynamics of the Solar Corona
NASA Space Physics Theory Contract NAS5-96081

5. FUNDING NUMBERS
C-NAS5-96081
PR-01-0157-07-7650-000

6. AUTHORS First Year Progess Report

Zoran Mikic

7. PERFORMING ORGANIZATION NAME(S) AND ADDRESS(ES)
Science Applications International Corporation
Mail Stop C2
10260 Campus Point Drive
San Diego, CA 92121-1578

8. PERFORMING ORGANIZATION REPORT NUMBER
SAIC-98/1031:APPAT-202

9. SPONSORING/MONITORING AGENCY NAME(S) AND ADDRESS(ES)
National Aeronautics & Space Administration
Goddard Space Flight Center
Greenbelt, MD 20771

10. SPONSORING/MONITORING AGENCY REPORT NUMBER

11. SUPPLEMENTARY NOTES

12a. DISTRIBUTION/AVAILABILITY STATEMENT

12b. DISTRIBUTION CODE

13. ABSTRACT *(Maximum 200 words)*

This report details progress during the first year of funding for our Space Physics Theory contract.

14. SUBJECT TERMS
solar corona
magnetohydrodynamics
numerical simulation
active regions

15. NUMBER OF PAGES
14

16. PRICE CODE

17. SECURITY CLASSIFICATION OF REPORT	18. SECURITY CLASSIFICATION OF THIS PAGE	19. SECURITY CLASSIFICATION OF ABSTRACT	20. LIMITATION OF ABSTRACT
UNCLASSIFIED	UNCLASSIFIED	UNCLASSIFIED	UL